A Liquid-State Theory of Dense Star Polymer Fluids

Christopher J. Grayce[†] and Kenneth S. Schweizer*

Departments of Materials Science & Engineering and Chemistry, and Materials Research Laboratory, University of Illinois, 1304 West Green Street, Urbana, Illinois 61801

Received July 5, 1995[⊗]

ABSTRACT: A liquid-state theory is presented for the conformational properties and intermolecular structure of concentrated solutions and bulk melts of purely repulsive star-branched polymers. The theory generalizes earlier work on linear chains and is based on a solvation potential, expansion of the single-chain free energy to second order in monomer interactions, and interaction-site integral equation theory. Information about the chemical structure of polymers, in particular intra- and intermolecular interaction potentials with a finite excluded volume per monomer, may be included straightforwardly. The theory does not assume incompressibility in the melt and suffers no loss of accuracy in the short-chain, small-arm-number limit. Also presented here is a study of conformational properties, including radius of gyration, mean arm end-to-end distance, monomer density profile, and local persistence length, for concentrated solutions and melts of a hard-sphere, branched-pearl-necklace model of star polymers with a moderate (4–12) number of arms. Stretching of the star arms near the branch point is found, and a concomitant swelling of the star with respect to the fully ideal state is predicted, even at meltlike densities and even in the few-arm limit. Measures of the swelling are compared with experimental measurements, the Daoud–Cotton "blob" model, and the "exclusion zone" model of Boothroyd and Ball. The physical origin of the stretching is also discussed in detail.

I. Introduction

Motivation for the study of star-branched polymers is partly abstract: polymers of nearly any architecture are composed of linear chain segments joining branch points, and an eventual understanding of the general relationship between polymer architecture and material properties would presumably owe much to the understanding of the simplest molecule that possesses both components. Motivation for the study is also partly practical: branched polymers have thermodynamic and particularly viscoelastic properties that are very different from those of their linear counterparts,[1,2] and in general a variation of polymer architecture leads to a strong variation of material properties. To the extent this variation is made predictable, it plays a role in the invention of new materials that is complementary to the (challenging) search for polymeric materials of new chemical identity. Extraction of general insights into the behavior of linear chains "tethered" at one end to a sharply-curved surface is also useful in a broader context including sterically-stabilized colloids,[3] diblock copolymer micelles,[4] end-associating functionalized polymers,[5] and "hairy molecular objects."[6]

Star polymers have been studied experimentally by rheology,[2,7,8] light scattering,[9–13] and small-angle neutron scattering (SANS).[10,11,14–17] Parallel theoretical study has used a local "blob" model,[18,19] scaling arguments,[18,20] renormalization-group theory,[21,22] self-consistent field theory,[23–25] computer simulation,[26–30] and several different semiempirical approaches.[31–35]

In all of these studies, with the exception of computer simulation, it is difficult or impossible to calculate directly and quantitatively the effects of the finite volume occupied by each monomer and the associated local packing constraints and liquid structure that occur at high polymer concentrations. While this limitation does not apply to computer simulations, simulations are confined at present to a single large star[26,27,29] or solutions of very small (oligomeric) stars[28] by the enormous expense of simulating solutions of large stars.[30]

What we present here is a theoretical approach to star polymer solutions that is complementary to other theoretical methods, because the effects of realistic monomer–monomer interaction potentials, expressing the full intra- and intermolecular excluded-volume interaction, may be studied in detail without the computational investment of a full-scale, many-molecule computer simulation. The effects of local and nonuniversal, system-specific chemical detail, such as monomer size and shape or local restrictions on chain flexion (chain stiffness), can also be straightforwardly studied.

Our method is a generalization of earlier work on linear chains[36–38] and makes use of interaction-site liquid-state integral equations developed by Chandler and Anderson[39–41] for the study of high-density fluids of small molecules and later extended by Curro and Schweizer[42,43] to polymeric fluids. In addition to presenting the theory itself, we also present in this paper a study, using a simplified athermal model, of some of the effects on star polymer conformation caused by changing molecular weight N, number of branches f, and polymer concentration ρ in concentrated solutions and in the melt. Conformational properties of common interest, such as the radius of gyration R_g, the mean distance R between the center and end of each arm, the intramolecular monomer density profile $\rho_{intra}(r)$, the local persistence length ξ, and the average intramolecular structure factor $\omega(k)$ are calculated. We also calculate the usual ratios g, g_{arm}, etc. expressing the difference between the size of star and linear polymers of the same weight and compare to values suggested by the Daoud–Cotton local-blob model,[18] the Boothroyd–Ball exclusion-zone model,[32] and experimental measurements in the melt state.[14]

We find in general that the model star molecules exhibit significant stretching of their arms near the branch point and that this stretching grows strongly with f and slowly with arm length N_a. This stretching of linear chains near a point of attachment is already familiar for *many*-arm stars in their incarnation as

[†] Present address: Department of Chemistry, University of California, Irvine, CA 92717.

[⊗] Abstract published in *Advance ACS Abstracts,* October 1, 1995.

0024-9297/95/2228-7461$09.00/0

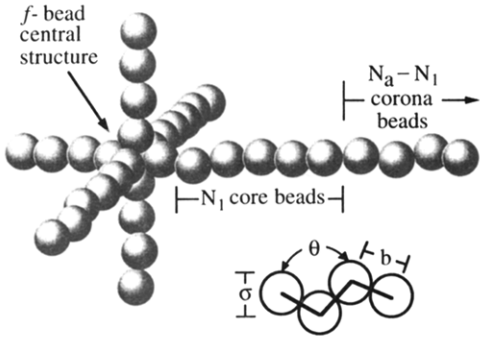

Figure 1. The star-branched pearl-necklace model. This is an "$f \times N_a$" star, meaning it has f arms ($f = 6$ here) and N_a sites per arm. The total molecular weight $N = f \times N_a + f$. Some number N_1 of sites on each arm are "core" sites, N_1 being determined variationally as described in the text. Note the definition of the angle θ between the bonds connecting next-nearest-neighbor (n.n.n.) sites.

polymer "brushes" on sharply-curved convex surfaces,[23,25,30] and it has in fact been proposed by previous workers to persist even to the few-arm limit, and even under Θ or melt conditions.[11,14,32,35] Our calculations support this somewhat surprising thesis.

Since the arm stretching is predicted and not assumed in our calculations, we can analyze its microscopic cause. This cause is the failure of certain excluded-volume interactions to be fully screened in the star at meltlike densities. Interestingly, the unscreened excluded-volume interactions involved are mostly between the outer portions of the star and the inner, and between outer portions on different branches. Thus we find it is more conceptually correct to imagine the star arms being "pulled" outward by the interactions the outer portions of the arms experience than to imagine the star arms being "pushed" out by the interactions the inner portions of the arms experience. There are two reasons why these excluded-volume interactions are not fully screened. The first is that shielding of the inner portions of the star by the outer leads to a reduction in the influence of the solvent upon the former. The second reason is that excluded-volume interactions between monomers are inherently less well screened when the monomers are weakly correlated with each other, and as noted the major influence on the interior of the star is interactions between monomers separated by long stretches of polymer backbone.

In what follows we first introduce in section II a model star polymer fluid. This allows concreteness in the description following, in section III, of a liquid-state, integral-equation based theory for the study of star polymer fluids. Although we discuss this theory in the context of the model described in section II, the theory is actually applicable without significant changes to much more complicated models for branched polymer solutions. The study of the specific model studied in this work is presented in section IV, and we conclude in section V. In a succeeding paper[44] we will present the calculated intermolecular properties of the model star fluid, including the density-fluctuation correlation functions that are measured by labeled light and neutron scattering experiments.

II. Model Star Polymer Fluid

We define a basic model of a star molecule that is a generalization of the "pearl-necklace" model of linear polymers studied earlier.[37] Attached to a branch point are f linear "pearl-necklace" chains of N_a backbone sites each (see Figure 1). We refer to this as an "$f \times N_a$" star. The spherical sites have diameter σ and are joined by rigid bonds of length b. The branch point consists of a rigid central structure built of f sites located at the vertices of a regular polyhedron of edge length b. Thus for the values $f = 4$, 6, 8, and 12 studied in section IV the central structure consists of sites at the vertices of a regular tetrahedron, octahedron, cube, and dodecahedron, respectively. The central structure for $f = 6$ is shown in Figure 1. The use of the f-vertex polyhedron as a central structure instead of the more common single site has no particular significance, but is made just for computational convenience. Note that the total number of sites N on the star is $fN_a + f$ and not fN_a.

The freedom of the molecule to bend and twist at each site may be restricted locally by a bending or torsional potential. For example, we can impose this simple local bending potential,

$$V_{bend}(\theta) = |\epsilon_0| + \epsilon_0 \cos\theta \tag{1}$$

where θ is the angle formed by neighboring bonds (see Figure 1), and ϵ_0 is a parameter controlling the strength and general effect of the potential. Values of $\epsilon_0 > 0$ favor large angles between neighboring bonds, and hence open chain conformations, while values of $\epsilon_0 < 0$ favor small angles between neighboring bonds and more compact chain conformations.[45] Including V_{bend} in the intramolecular interactions of the model star molecule is a first step toward a more realistic (nonuniversal) model of a star polymer. Appropriate values of ϵ_0 capture local chain stiffness resulting from the chemical bonding structure of the actual polymer of interest. Note that the competing effects of local chain stiffness and compression by the solvent would in general be expected to lead to complex conformational behavior. We will formulate our theory throughout for the general case of $\epsilon_0 \neq 0$, but in the study presented in section IV we will discuss results only for the simplest case of $\epsilon_0 = 0$.

Each of the sites on the star molecule interacts with all other sites on the same or on different molecules via a pairwise-additive, spherically symmetric site−site potential $u(r)$. In section IV we take $u(r)$ to be the purely repulsive hard-sphere potential,

$$u_{HS}(r) = \begin{cases} \infty; & r < \sigma \\ 0; & r \geq \sigma \end{cases} \tag{2}$$

where σ is the diameter of a site. The theory needs no significant modification for other purely-repulsive potentials (e.g., shifted-truncated Lennard-Jones).

The reason for neglecting the weak attractive forces between monomers at this stage is twofold: First, we are concerned here and in the next paper primarily with the *structural* properties of dense star fluids, in particular the average size and shape of the star molecules, the correlations between sites on different stars, and the density-fluctuation correlation functions measured by scattering experiments. The structure of fluids, in contrast to their thermodynamic and phase properties, appears at high density and temperature to be determined almost entirely by the strong short-range repulsive interactions in the fluid,[46,47] which $u_{HS}(r)$ adequately represents at this stage.

Our second reason for neglecting the attractions is that liquid-state theories can often relate, by relatively simple formulas, thermodynamic and phase properties of realistic model fluids, characterized by *both* attractions and repulsions, to the structural properties of

"reference" fluids characterized by repulsions only.[46] Thus the ability to calculate the structural properties of a "reference" hard-sphere star fluid is actually a necessary starting point for treating accurately fully realistic models of polymer fluids.[48,49]

Our model fluid consists of only the model star molecules at a number density ρ. That is, we do not consider explicitly a small-molecule solvent. If we wish to interpret a high-ρ fluid as a "melt" of the model stars, and lower-ρ fluids as "concentrated solutions" of the model stars—as we do—then we must assume the average influence of the small-molecule solvent has been included in the site−site potential; that is, $u(r)$ must represent an "effective" solvent-mediated interaction between the sites of the model star. Since in the present study we use $u(r) = u_{HS}(r)$, the small-molecule solvent implicit in our lower-ρ fluids must be a good solvent. Incidentally, there is no barrier other than the extra computational work involved to the explicit inclusion of a small-molecule solvent in the star polymer solution.

The density of the solution we express not in terms of the (small) molecular number density ρ but rather in terms of the monomer packing fraction η, which gives the fraction of space filled by the sites. For a solid of hexagonally-close-packed identical spheres $\eta = 0.74$, while the crystallization of a simple fluid of hard spheres occurs around $\eta = 0.49$.[50] As in ref 37, we will regard $\eta = 0.55$ as approximating roughly the density of a bulk melt of these hard-sphere stars, so that $\eta = 0.20$, the lowest density we investigate, corresponds in a rough sense to a 36% volume fraction polymer solution. For the tangent-site ($b = \sigma$) molecules we investigate in section IV, the packing fraction is simply related to the molecular number density,

$$\eta = \frac{\pi}{6} N \rho \sigma^3 \tag{3}$$

III. Theoretical Method

Our method is based on interaction-site integral-equation theory,[39-43] which describes the structure of the star polymer fluid at the level of the two-body site-pair correlation functions. These correlation functions are of two types: those we label $\omega_{\alpha\beta}(r)$ give the probability density that two sites α and β on the *same* molecule are a distance r apart. Those we label $g_{\alpha\beta}(r)$ give the probability density that two sites α and β on *different* molecules are a distance r apart, divided by the equivalent probability density for the ideal gas, which is just the total monomer density $N\rho$.

With these correlation functions we can answer structural questions such as the following: what is the probability that the centers of two star molecules A and B are separated by a distance R_{AB}? What is the probability that the end of a star arm is located a distance R from the star center? Of the sites that are the nearest neighbors to a particular site α, how many belong to the same molecule as α, and how many belong to other molecules? What are the partial and total scattering intensities as a function of scattering wavevector?

We cannot answer structural questions, on the other hand, that require three-site or higher correlation functions, such as: what are the angular correlations between star molecules—do the arms interleave like gear teeth at high density? What is the probability that two monomers α and β are both located to one side of the star center?

Our method was presented for linear chains in refs 36 and 37, and we refer the reader there for the complete derivation of the theory. We will only present in the next two sections the modifications to the theory required by the branched nature of the star polymer.

A. Intermolecular Theory. The intermolecular site-pair correlation functions $h_{\alpha\beta}(r) \equiv g_{\alpha\beta}(r) - 1$ are calculated from the intramolecular site-pair correlation functions $\omega_{\alpha\beta}(r)$ and the site−site potential $u(r)$ by the Polymer Reference Interaction-Site Model (PRISM) theory.[42,43] The only important change we need to make for the star fluids from the PRISM theory used for linear-chain fluids in ref 37 is to relax the "equivalent-sites" or "preaveraging" assumption. This assumption reduces the $\mathcal{O}(N^2)$ RISM equations to a more tractable number by aiming at the calculation not of each and every $h_{\alpha\beta}$, but of rather only the averages of the $h_{\alpha\beta}$ over the sites in each of several given regions of the molecule. That is, if we define P distinct regions of the molecule, to which belong $n_i \leq N$ ($i = 1...P$) sites each, then we calculate only the $P^2 \ll N^2$ site-averaged correlation functions h_{ij},

$$h_{ij}(r) \equiv [n_i n_j]^{-1} \sum_{\alpha=1(i)}^{n(i)} \sum_{\beta=1(j)}^{n(j)} h_{\alpha\beta}(r) \tag{4}$$

where 1(i) is the label of the first, and $n(i)$ the label of the last site in region i. The h_{ij} can be calculated from P^2 similarly-defined site-averaged ω_{ij} by means of only $\mathcal{O}(P^2)$ PRISM equations if the "equivalent-sites" approximation is made. This approximation sets all of the $n_i \times n_j$ "direct" correlation functions $c_{\alpha\beta}$ for sites α,β in the averaging regions i,j equal to the *same* function c_{ij}, i.e.

$$c_{\alpha\beta}(r) \approx c_{ij}(r); \quad \alpha = 1(i)...n(i), \quad \beta = 1(j)...n(j) \tag{5}$$

The equivalent-sites approximation is made in the expectation that the $c_{\alpha\beta}(r)$, being very short-ranged in r, will be insensitive to variations on a large length scale of the chemical bonding structure of the molecule—such as the fact that it has ends. It is only these variations that distinguish one site in a homopolymer from another.[42]

In our earlier linear-chain work[37] we were concerned about only the totally averaged behavior of the molecule—e.g., its radius of gyration, the totally averaged intermolecular pair correlation function $g = N^{-2} \sum_{\alpha,\beta} g_{\alpha\beta}$ or the total collective scattering function $S(k)$. Thus we set $P = 1$, replacing *all* $c_{\alpha\beta}$ with *one* function c, and reducing the RISM equations to but one PRISM equation. In this work, however, it is precisely the "end effects"—or rather "branch-point effects"—in which we are interested, and we cannot set $P = 1$ without sacrificing entirely our ability to calculate these effects. On the other hand, we still expect eq 5 to be generally accurate, since the fact that a molecule has a branch point is also a variation in chemical bonding structure on a large length scale. That is, retaining the distinction between all N^2 of the $c_{\alpha\beta}$ is presumably still not necessary, so long as we do not ask questions about each individual $h_{\alpha\beta}$ but rather only about the averaged h_{ij}.

What we have done therefore is make a simple extension of the completely-equivalent-sites theory: we have taken $P = 3$, that is we have assumed that there are three types of site instead of just one. Type 0 sites are the f sites on the central structure of the star. Type 1 sites are the $f \times N_1$ sites in some inner "core" region

of each arm, and type 2 sites are the remaining $f \times (N_a - N_1)$ sites on each arm, which are in an outer "corona" region. The coarse division of monomer identity into "core" and "corona" types has been employed in many other theoretical descriptions of the star polymer.[18,25,35] We have separated additionally the central (type 0) sites from the core (type 1) sites, only because the intermolecular correlation function h_{00} is of special interest, since it gives directly the correlation between the centers of gravity of the star molecules. h_{00} will be discussed in a succeeding paper.[44]

The three-site-type approximation implies nine distinct correlation functions c_{ij}, of which only six are unique because of the general symmetry $c_{\alpha\beta} = c_{\beta\alpha}$. These enter nine coupled PRISM equations, of which again only six are unique by symmetry:

$$\mathbf{H}(k) = [\mathbf{1} - \rho\mathbf{\Omega}(k)\cdot\mathbf{C}(k)]^{-1}\cdot[\mathbf{\Omega}(k)\cdot\mathbf{C}(k)\cdot\mathbf{\Omega}(k)] \quad (6)$$

$$H_{ij}(k) = [n_i n_j]^{-1/2} \sum_{\alpha}^{n_i} \sum_{\beta}^{n_j} h_{\alpha\beta}(k)$$

$$\Omega_{ij}(k) = [n_i n_j]^{-1} \sum_{\alpha}^{n_i} \sum_{\beta}^{n_j} \omega_{\alpha\beta}(k)$$

$$C_{ij}(k) = [n_i n_j]^{+1/2} c_{ij}(k)$$

where $h_{\alpha\beta}(r) = g_{\alpha\beta}(r) - 1$, and we have written the equations in k-space, not distinguishing notationally between functions and their Fourier transforms (*cf.* eq 16 of ref 37).

Equation 6 must be supplemented by a closure approximation. We use the site–site Percus–Yevick closure approximation,[39,42]

$$c_{\alpha\beta}(r) = [1 - \exp\{\beta u(r)\}][h_{\alpha\beta}(r) + 1] \quad (7)$$

eqs 6 and 7 are solved numerically as in ref 37 by Picard iteration and fast Fourier transform. Each function c_{ij}, ω_{ij}, and h_{ij} is represented in r-space at 2^{14} points spaced 0.0125σ apart between $r = 0$ and $r = 204.8\sigma$, and thus in k-space at 2^{14} points, spaced $0.015\sigma^{-1}$ apart between $k = 0$ and $k = 251.3\sigma^{-1}$. Convergence is defined to be a change in the integrated difference of $rH_{ij}(r)$ from one iteration to the next of less than one part in 10^{-12}. Mixing of the H_{ij} from one iteration to the next is as usual necessary to ensure stability of the Picard process. By judicious choice of the mixing fractions, in particular by scaling the mixing fraction for each type with the relative number of sites of that type, solving eq 6 can be done in about the same number of Picard iterations as solving the single PRISM equation obtained for $P = 1$. For example, solving the 6 PRISM equations for a 3-region 8 × 100 star at $\eta = 0.55$ requires 2540 iterations, while solving the single PRISM equation for a single-region linear 808-mer at $\eta = 0.55$ requires 2007 iterations. Both calculations would be substantially faster, of course, at a lower density.

The density used in all our PRISM calculations is corrected in the usual way, described in ref 59, for the small (typically 3–4%) intramolecular overlap associated with the use of $\omega_{\alpha\beta}(r)$ that are not uniformly zero for $r < \sigma$.

B. Intramolecular Theory. The intramolecular pair correlation functions $\omega_{\alpha\beta}$, which describe the conformation of a single molecule, are profoundly influenced at high polymer concentrations by the intermolecular interactions. Determining $\omega_{\alpha\beta}$ at high density is therefore a priori a strongly many-molecule problem. We may formally replace this many-molecule problem, however, with an exactly equivalent single-molecule problem by use of a fictitious "solvation" potential W.[36,51] W is constructed such that the conformational properties of an *isolated* molecule experiencing the extra potential W are equivalent—in principle exactly—to the conformational properties of the same molecule interacting with all the other molecules in a high-density solution.

How to construct the exact solvation potential is unfortunately not yet known. Some methods for calculating a pairwise-additive approximation to W from the intermolecular pair correlations $h_{\alpha\beta}$ were presented in ref 36. Further discussion, including some of the limitations of solvation potentials based on RISM theory, was presented in ref 38. Earlier PRISM-based work involving different approaches can be found in refs 52 and 53. The same ideas have also found use in calculations of intermolecular correlations in molecular fluids[54] and the density inhomogeneity induced in a polymer fluid by an impenetrable surface.[55,56]

We use here the Percus–Yevick-style pairwise-additive approximate solvation potential derived in ref 36, which has been argued[37,38] to be the most accurate presently known for interaction-site fluids with a short-range site–site interaction $u(r)$. The only difference between the appearance of W in this work and in ref 37 is the presence here of nine different pair-components W_{ij}, of which six are unique,[57] corresponding to the nine (six unique) direct correlation functions,[58]

$$W[\mathbf{r}_1 \ldots \mathbf{r}_N] = \sum_{\alpha=1}^{N-1} \sum_{\beta=\alpha-1}^{N} W_{ij}(|\mathbf{r}_\alpha - \mathbf{r}_\beta|) \quad (8)$$

$$\beta W_{ij}(r) = -\ln[1 + \rho \sum_{k,l=0}^{2} \int \mathrm{d}^3 r_s \, \mathrm{d}^3 r_{s'} \, c_{ik}(|\mathbf{r} - \mathbf{r}_s|) S_{kl}(|\mathbf{r}_s - \mathbf{r}_{s'}|) c_{lj}(r_{s'})]$$

where $\{\mathbf{r}_1 \ldots \mathbf{r}_N\}$ locate the N sites of the star molecule, β is inverse temperature, and i and j are the site-types (0, 1, or 2) of the sites α and β (*cf.* eq 9 of ref 37). The S_{ij} are the partial structure factors or partial density autocorrelation functions of the fluid (*cf.* eq 11 of ref 37).

The $\omega_{\alpha\beta}$ of the star in high-density solution are determined by finding the equivalent quantities for the star experiencing W in addition to the "bare" intramolecular potential V_1,

$$\omega_{\alpha\beta}(r) = Z_1^{-1} \int \mathrm{d}\mathbf{r}_1 \ldots \mathrm{d}\mathbf{r}_N \, \delta(\mathbf{r} - |\mathbf{r}_\alpha - \mathbf{r}_\beta|) s_N^{\mathrm{eq}}(\mathbf{r}_1 \ldots \mathbf{r}_N) \quad (9)$$

$$s_N^{\mathrm{eq}}(\mathbf{r}_1 \ldots \mathbf{r}_N) = \exp\{-\beta(V_1 + W)\}$$

$$V_1 = \sum_{\alpha<\beta}^{N} u(|\mathbf{r}_\alpha - \mathbf{r}_\beta|) + \sum_{\substack{\text{n.n.n.} \\ (\alpha,\beta)}} V_{\mathrm{bend}}(\theta_{\alpha\beta};\epsilon_0) \quad (10)$$

where the constant Z_1 normalizes s_N^{eq}, the equilibrium probability distribution of single-chain conformations, to unity, and the second sum in V_1 is taken over all pairs of sites α and β that are next-nearest neighbors ("n.n.n.") along the chain.

The direct method of calculating the right-hand side of eq 9 is a statistical evaluation of the integral, i.e. a Monte-Carlo computer simulation of the single molecule

experiencing the potential $V_1 + W$. This would be far more expensive for the star molecules studied here that it was for the linear molecules studied in ref 37, because the stars here are from 4 to 200 times as big as the largest of the linear chains we considered earlier. However, we also developed in ref 37 an approximate variational method for calculating the equilibrium $\omega_{\alpha\beta}$, which produced results at high density as good or better than those from the Monte-Carlo method. We will use this second approach here. This requires an expression for a "trial" equilibrium probability distribution function s_N and a generating function $F[s_N]$, the minimization of which defines the equilibrium distribution s_N^{eq}.

For the trial distribution function we use a generalization of eqs 25 and 26 of ref 37,

$$s_N(\mathbf{r}_1...\mathbf{r}_N) = \tilde{Z}_1^{-1} \exp\{-\beta \tilde{V}_1\} \tag{11}$$

$$\tilde{V}_1(\mathbf{r}_1...\mathbf{r}_N) = \sum_{\substack{\text{n.n.n.} \\ (\alpha,\beta)}} u(|\mathbf{r}_\alpha - \mathbf{r}_\beta|) + V_{\text{bend}}(\theta_{\alpha\beta};\epsilon_{\alpha\beta})$$

where the (many) variational parameters $\epsilon_{\alpha\beta}$ determine the (possibly different) degrees of local chain expansion or contraction at each n.n.n. bending degree of freedom in the trial conformation. V_{bend} is chosen to have the same form as the actual n.n.n. bending potential of the model star molecule, eq 1. (But note that this does not imply any *a priori* relationship between ϵ_0, the parameter that defines the local stiffness of the *real molecule*, and the $\epsilon_{\alpha\beta}$, which define the degree of expansion or effective local stiffness of the *trial conformation*). The bonding constraints are taken into account by constraining the form of s_N to be that appropriate for a connected polymer rather than by introducing an explicit potential between bonded sites into $\tilde{V}_1$.

For the generating functions $F[s_N]$ we also generalize the results of ref 37. Employing the same virial expansion and truncation at pair interactions, and with the use of eq 11, we can write the following generalization of eq 33 of ref 37,

$$F(\{\epsilon_{\alpha\beta}\};\{\epsilon_{\alpha\beta}^{eq}\}) = F_{\text{ideal}} + F_{\text{exc}} + F_{\text{solv}} \tag{12}$$

$$\beta F_{\text{ideal}} = -\sum_{\substack{\text{n.n.n.} \\ (\alpha,\beta)}} \log Z_\theta(\epsilon_{\alpha\beta}) + \beta \int_0^\infty \mathrm{d}r\, 4\pi r^2\, \omega_{\alpha\beta}(r)[V_{\text{bend}}(\theta_{\alpha\beta};\epsilon_{\alpha\beta}) - V_{\text{bend}}(\theta_{\alpha\beta};\epsilon_0)]$$

$$\beta F_{\text{exc}} = -\sum_{\alpha+2<\beta} \int_0^\sigma \mathrm{d}r\, 4\pi r^2 \omega_{\alpha\beta}(r)\, [\exp\{-\beta u_{\text{HS}}(r)\} - 1]$$

$$\beta F_{\text{solv}} = -\sum_{\alpha+2<\beta} \int_\sigma^\infty \mathrm{d}r\, 4\pi r^2\, \omega_{\alpha\beta}(r)[\exp\{-\beta W_{\alpha\beta}(r;\epsilon_{\alpha b}^{eq})\} - 1] + \sum_{\substack{\text{n.n.n.} \\ (\alpha,\beta)}} \int_0^\infty \mathrm{d}r\, 4\pi r^2 \omega_{\alpha\beta}(r)\, \beta W_{\alpha\beta}(r;\epsilon_{\alpha\beta}^{eq})$$

$$Z_\theta(\epsilon) = \int_{-1}^{1} \mathrm{d}(\cos\theta) \exp\{-\beta u_{\text{HS}}(b[2 + 2\cos\theta]^{1/2}) - \beta V_{\text{bend}}(\theta;\epsilon)\}$$

where each of the $\omega_{\alpha\beta}$ on the right-hand side of this equation depends a priori on *all* of the variational parameters $\epsilon_{\alpha\beta}$. There are minor notational differences between this expression and eq 33 of ref 37: We have written here $\omega_{\alpha\beta}$ instead of $s_2^{\alpha\beta}$; there is no difference as long as $\alpha \neq \beta$, as it does everywhere in eq 12. We have also kept a term in F_{ideal} that depends on ϵ_0, which we dropped in ref 37 because we considered there only $\epsilon_0 = 0$, and we have dropped the n.n.n. terms in F_{exc}, which are always zero for trial conformations given by eq 11.

The significant difference between $\tilde{V}_1$ and F as used here and in ref 37 is that there are of order N variational parameters $\epsilon_{\alpha\beta}$ describing a unique effective stiffness for each n.n.n. pair. It is not practical to keep all of these parameters independent, nor would it be logically consistent: There are only three site types as far as the solvation potential pair components W_{ij} are concerned, and therefore only five potential types of n.n.n. pairs as far as intermolecular interactions are concerned: pairs in regions 0, 1, and 2, and "junction" pairs straddling regions 0 and 1 or 1 and 2.

There is no need for a variational parameter for pairs in region 0 (the central structure), because these sites are fixed relative to one another and cannot respond to interactions with other sites. There would also appear to be little need for independence in the stiffness parameters of the small number (of order f/N) of junction pairs. The most logical approach would be to define a mixing rule that equates the stiffness parameter of each junction pair to some average of the stiffness parameters of the two regions it straddled. But we have not done this. The convolution approximation described below (eq 13) that allows us to calculate easily the pair correlation function between sites in different regions necessarily implies that all the stiffness parameters of the junction sites are set to zero. One would expect this to be a relatively unimportant consequence so long as the star arms are quite flexible, because while inserting a freely-jointed link would drastically change the conformational properties of a rigid rod, it would not significantly change the properties of a flexible coil.

We are left, therefore, with two independent stiffness parameters, ϵ_1 for the core n.n.n. pairs on each arm, and ϵ_2 for the corona n.n.n. pairs. These two, along with the number N_1 of sites on each arm that are defined to be in the core, are the three variational parameters that determine the trial star conformation s_N via eq 11. The functional minimization of $F[s_N]$ is then obtained by the ordinary minimization of $F(\epsilon_1,\epsilon_2,N_1)$.

To calculate the trial intramolecular pair correlations $\omega_{\alpha\beta}$ that enter eq 12 we use the discrete Koyama semiflexible chain approximation.[59] We calculate the n.n.n. correlations $\omega_{\alpha\alpha+2}$ exactly. For the case of n.n.n. pairs where one site lies on the central structure this involves some nontrivial but straightforward analytic geometry.

With three site types we must specify how to calculate $\omega_{\alpha\beta}$ when sites α and β lie in different regions. For simplicity we have made a "Markov" convolution approximation,

$$\omega_{\alpha\beta}(|\mathbf{r}_\alpha - \mathbf{r}_\beta|) = \int \mathrm{d}^3 r_J \omega_{\alpha J}(|\mathbf{r}_\alpha - \mathbf{r}_J|)\omega_{J\beta}(|\mathbf{r}_J - \mathbf{r}_\beta|) \tag{13}$$

for sites in neighboring regions, e.g. 0 and 1 or 1 and 2 on the same arm. The site J is the junction site between the two regions, and as mentioned above, eq 13 implies that the stiffness parameters for the two n.n.n. pairs of which J is a member are both zero.

When α and β are in nonneighboring regions (e.g. 0 and 2 on the same arm, or any two regions on different

arms) we use the obvious multiple-convolution extension of eq 13, involving sites J, J', etc. that lie at the junctions of the regions lying between α and β, and involving integrations over $\mathbf{r}_J$, $\mathbf{r}_{J'}$, etc.

F depends, as in ref 37, not only on the trial values of the variational parameters $\epsilon_{\alpha\beta}$ but also parametrically on the equilibrium values of these parameters $\epsilon_{\alpha\beta}^{eq}$, because it is the $\epsilon_{\alpha\beta}^{eq}$ that determine the solvation potentials $W_{\alpha\beta}$. Thus finding the $\epsilon_{\alpha\beta}^{eq}$ from F is a self-consistent process: We guess an initial set and calculate from them a set of equilibrium intramolecular correlation functions $\omega_{\alpha\beta}$. We use the $\omega_{\alpha\beta}$ and PRISM theory (eq 6) to calculate the intermolecular pair correlation functions $c_{\alpha\beta}$ and $S_{\alpha\beta}$, and then use eq 8 to form the solvation potentials $W_{\alpha\beta}$. Inserting the $W_{\alpha\beta}$ into F, we then minimize F with respect to the $\epsilon_{\alpha\beta}$, and this provides a new, better set of values for the $\epsilon_{\alpha\beta}^{eq}$. We continue the recursion until the set of equilibrium variational parameters we use to calculate $W_{\alpha\beta}$ is the same as the set we find by minimizing F. We require exact self-consistency for the integer number N_1^{eq} and typically consistency within one part in 10^3 for the real numbers ϵ_1 and ϵ_2. This takes 5−7 recursive minimizations of F. The recursion is apparently stable, and "mixing" of the variational parameters from the $(i-1)$th and ith iteration is not required.

It is possible to interpret the self-consistent minimization process physically: Minimization of F corresponds to minimizing, with respect to the probability distribution of conformations, the effective single-molecule free energy of a "test" star molecule inserted into the solvating medium of the other star molecules.[60] The solvation potentials $W_{\alpha\beta}$ describe the influence on the test star of the solvating medium. This influence quite naturally depends on the conformational properties of the stars in the medium, which is expressed by the dependence of $W_{\alpha\beta}$ on the equilibrium values of the conformational variational parameters $\epsilon_{\alpha\beta}^{eq}$. The self-consistency condition is then the physical requirement that, since they are all physically identical, the parameters describing the conformation of the solvating stars must be the same as those describing the conformation of the test star.

From this physical point of view there are three distinct contributions to F, indicated explicitly in eq 12 as F_{ideal}, F_{exc}, and F_{solv}, and which have the following interpretations.

F_{ideal} measures the "ideal" free energy of the test star, the free energy of the star due only to the bonding constraints and the local intramolecular interactions. We have defined the "local" interactions to be just the excluded-volume and bending-potential interactions between n.n.n. sites. We have also chosen the local interactions determining the trial conformational distribution function s_N to have the same form as the local interactions of the real star; in particular we chose $V_{bend}(\epsilon_{\alpha\beta})$ in $\tilde{V}_1$ to have the same form as the n.n.n. bending potential of the actual star, as given by eq 1. Thus the minimum of F_{ideal} occurs simply when $\epsilon_{\alpha\beta} = \epsilon_0$, and F_{ideal} rises if any of the $\epsilon_{\alpha\beta} \neq \epsilon_0$.

F_{exc} measures the free energy arising from the long-range intramolecular excluded-volume forces. That is, it measures at the level of the second monomeric virial coefficient the entropy loss of the chain due to the restriction that the monomers not overlap. F_{exc} rises with more compressed trial conformations and falls with more expanded trial conformations.

Table 1. Equilibrium Conformational Parameters for Various Stars

$f \times N_a$	η	ϵ_1^{eq}	ϵ_2^{eq}	N_1^{eq}	$\langle\theta\rangle_1$[a] (deg)	$\langle\theta\rangle_2$[b] (deg)	R_1^2/σ^2[c]
4 × 100	0.20	1.65	0.73	10	122	113	24.6
4 × 100	0.55	1.33	−0.025	6	119	104	10.8
8 × 100	0.20	2.80	0.77	13	132	113	47.9
8 × 100	0.55	2.37	0.044	10	128	105	30.1
8 × 1600	0.20	4.10	0.88	21	139	114	120
8 × 1600	0.55	3.38	0.15	17	136	106	78.4
12 × 100	0.20	3.65	0.78	15	137	113	70.5
12 × 100	0.55	3.13	0.065	12	134	105	46.4

[a] Average n.n.n. angle in core region (see Figure 1). [b] Average n.n.n. angle in corona region. [c] Mean square length of core region.

F_{solv} measures the free energy cost of the intermolecular packing constraints, as conveyed by the solvation potential. F_{solv} rises with more expanded trial conformations, reflecting the need in expanding the star to push against the solvent, and rises with density, as the strength of the solvation potential itself grows (see Figure 15 below).

We may define a test star that is ideal in the usual Flory sense, i.e. a star for which the long-range forces cancel and $F_{exc} + F_{solv}$ equals a constant independent of conformation. The equilibrium distribution of conformations for this star is that which minimizes F_{ideal} alone, i.e. $\epsilon_{\alpha\beta} = \epsilon_0$. Note that this ideal distribution of conformations depends only on ϵ_0 and is independent of polymer concentration. In the general case $F_{exc} + F_{solv}$ does depend on conformation and the test star can reduce this net nonideal free energy by moving away from the ideal distribution of conformations. This increases F_{ideal}, and so the equilibrium distribution of conformations is in a general sense determined by the trade-off between the "cost" of increasing F_{ideal} and the "benefit" of decreasing $F_{exc} + F_{solv}$. The balance point will vary with polymer concentration.

IV. Conformation of Model Stars in Solution

Using the method presented in section III, we have studied the conformational changes in the model stars defined in section II, changes that are induced by changing solution density, number of star arms f, and length of arms N_a. We have taken $b = \sigma$, that is, the sites in the star molecular are just tangent, and set $\epsilon_0 = 0$, that is the stars have no local stiffness. This is exactly the model that has been studied most extensively in off-lattice computer simulations of the single star.[30] Our work is complementary, therefore, to the existing computer simulation work, because we study the (otherwise inaccessible) case of *high* polymer concentration with the same basic model.

The principal results of our calculations are presented in several figures and tables, as follows: Table 1 shows the equilibrium values of the variational conformational parameters $\{\epsilon_1^{eq}, \epsilon_2^{eq}, N_1^{eq}\}$ for some typical stars. All stiffness parameters are measured in units of k_BT. Note that the equilibrium stiffness parameters for the core sites are always higher than those for the corona sites and that the disparity increases with density, arm length and arm number.

Figure 2 shows the variation in star radius of gyration R_g with polymer concentration, as measured by monomer packing fraction η, across the "concentrated" regime and into the "melt" for $f \times 100$ stars. We find R_g decreases smoothly with η for all stars, and the total decrease over the range shown ($0.20 \leq \eta \leq 0.55$) is about 20%. This general behavior is the same as that calcu-

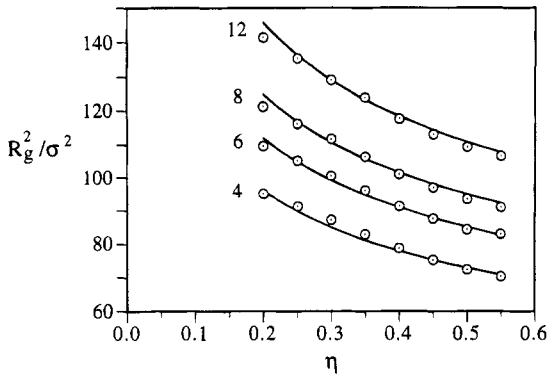

Figure 2. Squared radius of gyration R_g^2 of $f \times 100$ stars as a function of monomer packing fraction η. Each set of points is marked with the value of f. The curves are $35.0f^{0.38}\eta^{-0.30}$.

Table 2. Size of 8 × N_a Star Molecules at "Concentrated Solution" Densities (η = 0.20)

	arm length N_a				
measure[a]	100	200	400	800	1600
R^2/σ^2	243	491	981	1954	3885
g_{arm}	1.18	1.14	1.11	1.08	1.06
R_g^2/σ^2	121	239	470	922	1815
g	0.398	0.390	0.381	0.371	0.364
$g - g_0$	0.057	0.047	0.038	0.028	0.020
$(g - g_0)/g_0$	0.17	0.14	0.11	0.08	0.06
c^2/σ^2	20	29	40	53	69

[a] Apparent power laws: $g \sim N_a^{-0.034}$, $c^2 \sim N_a^{0.44}$.

lated in our earlier work for linear chains.[37] If we force a power-law dependency on $R_g^2(f,\eta,N_a = 100)$, we find a best fit with

$$R_g^2(f,\eta,N_a = 100) = 35.0f^{0.38}\eta^{-0.30} \qquad (14)$$

and this function has been used to draw the curves in Figure 2. The significance of the exponents is difficult to assess, since the range of f and η over which they have been extracted is small. Note, however, that $R_g^2 \sim \eta^{-0.25}$ is predicted by scaling arguments for the size of linear polymers in semidilute solution.[61] Figure 2 and eq 14 imply that contraction of star polymers with density is predicted by our theory to continue *throughout* the semidilute and concentrated solution regimes and on into the melt. (Indeed, no density-independent value of R_g ever appears in our calculations.) These results are consistent with our earlier results on linear chains,[37] and as discussed there with the few experimental measurements on linear chains that have been made. No contradiction of scaling arguments is implied by this—note that *by construction* $R_g^2 \sim N$ for all our stars in the $N \to \infty$ limit. Rather, as we observed earlier,[37] our results suggest that the effective segment size or persistence length that enters scaling arguments and similar "coarse-grained," long-wavelength theories as an unknown parameter is not independent of polymer concentration.

Tables 2 and 3 show how the size of 8-arm stars changes with arm length N_a at constant "concentrated solution" (η = 0.20) and "melt" (η = 0.55) densities. Tables 4 and 5 by contrast show how the size of stars with fixed arm length N_a = 100 changes with arm number f, also at η = 0.20 and η = 0.55. Shown in each of these four tables are also various ratios that have been used to quantify the differences observed between the sizes of stars and the sizes of linear chains, and between the sizes of real (or realistically-modeled) stars

Table 3. Size of 8 × N_a Star Molecules at "Melt" Densities (η = 0.55)

	arm length N_a				
measure[a]	100	200	400	800	1600
R^2/σ^2	180	364	728	1450	2882
g_{arm}	1.15	1.12	1.09	1.06	1.04
R_g^2/σ^2	91.0	179	349	684	1346
g	0.382	0.373	0.361	0.352	0.345
$g - g_0$	0.041	0.030	0.018	0.009	0.002
$(g - g_0)/g_0$	0.12	0.09	0.05	0.03	0.01
c^2/σ^2	15	21	28	37	48

[a] Apparent power laws: $g \sim N_a^{-0.038}$, $c^2 \sim N_a^{0.42}$.

Table 4. Size of f × 100 Star Molecules at "Concentrated Solution" Densities (η = 0.20)

	arm number f			
measure[a]	4	6	8	12
R^2/σ^2	222	233	243	261
g_{arm}	1.08	1.13	1.18	1.27
R_g^2/σ^2	95.0	110	121	141
g	0.638	0.484	0.403	0.307
$g - g_0$	0.017	0.043	0.062	0.073
$(g - g_0)/g_0$	0.03	0.10	0.18	0.31
c^2/σ^2	5.2	13	20	37

[a] Apparent power laws: $g \sim f^{-0.66}$, $c^2 \sim f^{1.8}$.

Table 5. Size of f × 100 Star Molecules at "Melt" Densities (η = 0.55)

	arm number f			
measure[a]	4	6	8	12
R^2/σ^2	163	174	180	194
g_{arm}	1.05	1.11	1.15	1.24
R_g^2/σ^2	70.3	83.0	91.0	106
g	0.603	0.469	0.401	0.296
$g - g_0$	−0.018	0.027	0.059	0.061
$(g - g_0)/g_0$	−0.03	0.06	0.17	0.26
c^2/σ^2	3.3	11	15	27

[a] Apparent power laws: $g \sim f^{-0.64}$, $c^2 \sim f^{1.9}$.

and the ideal Gaussian-chain model of stars:[62]

$$g_{arm} \equiv R^2/R_{(lin)}^2 \qquad (15)$$

$$g \equiv R_g^2/R_{g(lin)}^2 \qquad (16)$$

$$g - g_0 \equiv \frac{R_g^2}{R_{g(lin)}^2} - \frac{S_g^2}{S_{g(lin)}^2} \qquad (17)$$

$$c^2 \equiv R_g^2 - \tilde{R}_g^2 \qquad (18)$$

where $R_{(lin)}^2$ is the mean square end-to-end distance of a linear chain of length N_a, and $R_{g(lin)}^2$ is the mean square radius of gyration of a linear chain of length $N = fN_a + f$. S_g^2 and $S_{g(lin)}^2$ are the mean square radii of gyration of a Gaussian star and Gaussian linear chain, respectively, both of size N. Finally $\tilde{R}_g^2$ is the radius of gyration of a hypothetical star exactly like the real star except that ϵ_1 and ϵ_2 are set equal to ϵ_2^{eq}; i.e. this is a star in which the local chain expansion has been forced to be equal everywhere to the equilibrium local chain expansion calculated for the outer, corona region of the real star.

We calculate $R_{(lin)}^2$ using the same pearl-necklace model we have adopted for the stars, using the same generating functional theory, as it was presented in ref 37 for linear chains. We define S_g^2 to be the mean square radius of gyration of a star consisting of f

Gaussian chains of mean square step length b^2 attached to our central branch-point structure. That is, we have removed the trivial effects of the finite size and shape of our central structure, so that any difference between R_g^2 and S_g^2 reflects non-Gaussian behavior of the arms. For this definition the exact expression for S_g^2 is

$$S_g^2 = \frac{N}{6}\left\{\frac{(3f-2)N_a^2}{f^2(N_a+1)^2} + \frac{(3f-1)N_a}{f^2(N_a+1)^2} + \frac{3c_1N_a(N_a+2f)}{f^3(N_a+1)^3} + \frac{3c_2}{f^3(N_a+1)^3}\right\} \quad (19)$$

$$c_1 = \sum_{i=2}^{f}\langle(\mathbf{r}_i^{(0)} - \mathbf{r}_1^{(0)})^2\rangle$$

$$c_2 = 2\sum_{i=1}^{f}\sum_{j=i+1}^{f}\langle(\mathbf{r}_i^{(0)} - \mathbf{r}_j^{(0)})^2\rangle \quad (20)$$

where $\mathbf{r}_i^{(0)}$ is the location of the ith site of the center structure. In the long-arm limit, $N_a \to \infty$, only the first term on the right-hand side of eq 19 survives, and we recover for S_g^2 the customary expression for Gaussian stars,[62]

$$S_g^2 = \frac{N}{6}\left\{\frac{3f-2}{f^2}\right\} \quad (21)$$

The physical meaning of the measures in eqs 15–18 is as follows: g_{arm} quantifies the stretching of a linear chain that occurs when they are "tethered" together at one end in sets of f instead of being allowed to freely mix. g shows the overall contraction of the star relative to a linear molecule of the same total weight. Of course, much of this contraction is attributable simply to the increased connectivity of the star: eight 100-site chains with their ends tied together must occupy a smaller volume than one 800-site chain, so long as the chains fill space inefficiently. However, it turns out that the contraction due to increased connectivity is not fully realized, due to nonideal stretching of the star arms, as discussed more fully in section IV.C below. To quantify *this* effect, we have defined g_0, the equivalent of g for a purely Gaussian star and chain, and then show in Tables 2–5 both the absolute and relative difference between g and g_0. Since any piece of a Gaussian chain molecule has no interaction through space with any other piece of the same molecule, the arms of a Gaussian star are in no way different from linear chains of the same length. Values of g_0 not equal to unity can result then only from the effects of star connectivity, and so by comparing g_0 to g we compare the shrinkage of the star (relative to the linear chain) due only to star connectivity and the actual shrinkage of the star.

For example, from Table 4 g is 3% larger than g_0 for $f = 4$ stars at $\eta = 0.20$, indicating that 3% of the shrinkage expected from increased connectivity is not realized in the real star because of nonideal stretching in the arms. Or we could equivalently say that due to arm stretching, an expansion of the real star occurs that is 3% of the magnitude of the shrinkage due to the connectivity. For $f = 12$ stars the nonideal expansion is much larger and g rises to a value 31% larger than g_0.

The quantity c^2, like $g - g_0$, measures the expansion of the star relative to a star model with independent arms, but the latter is not the Gaussian-star model. Instead we have constructed a star exactly like our actual star, but with both core *and* corona stiffness parameters, ϵ_1 and ϵ_2, set equal to the corona stiffness parameter ϵ_2^{eq} of the actual star. What we have done by this choice is ensure that the chains that make up the independent-arm model star are identical along their entire length, and have the same properties at the branch point as they do far away, and have the same properties as the actual star arm has far from the branch point of the actual star. This prevents any contribution to c^2 from effects not related to the existence of the branch point, e.g. the fact that we predict a slow increase in local chain expansion with molecular weight for any architecture at these molecular weights. c^2 was defined in the general sense by Boothroyd and Ball[32] to classify models of star conformation, as we will discuss further in section IV.A.

At fixed N_a we find from Figure 2 that R_g increases with f at all densities, unsurprisingly. But this increase is larger than that predicted by the increase in star connectivity with f, as is shown by the increase in $g - g_0$ with f shown in Tables 4 and 5. The fact that this extra swelling of the star decreases with increased density (compare values of $g - g_0$ in Table 4 with values of $g - g_0$ in Table 5) suggests that its physical origin lies in incomplete screening of long-range intramolecular repulsion, because screening increases with density. The fact that the relative extra swelling decreases with arm length (see Tables 2 and 3) suggests that the important region in which incomplete screening occurs is near the branch point, because the relative contribution of this region to the size of the entire star decreases with arm length.

These suggestions can be tested by a more detailed picture of the changing star conformation. We define $\Delta\rho(r)$ to be the difference between the monomer density per arm of an $f \times N_a$ star and the monomer density of a linear chain of length N_a under the same conditions,

$$\Delta\rho(r) = f^{-1}\rho_{star}(r) - \rho_{chain}(r) \quad (22)$$

where r is measured from the center of the star and from the end of the linear chain. The purpose of this measure is, first, if the star were essentially like f linear chains at the same density connected together by their ends—and these chains would have some small residual nonideality even at high density[37]—then $\Delta\rho(r)$ would be identically zero. Secondly, since the total number of monomers on an arm and linear chain is the same, $\Delta\rho(r)$ must always integrate to zero, so that $\Delta\rho(r)$ highlights the changes in the radial *distribution* of monomer density as we go from lengths of chain that are free to lengths that form the arms of a star polymer.

Figure 3 shows $\Delta\rho(r)$ for varying f and η. Three effects are apparent. First of all, $\Delta\rho(r)$ is not flat. When f linear chains are joined to form a star, monomer density is transferred from the regions of the chains near the branch point to regions farther out. It is this transfer of density outward that causes the extra swelling of the star. Second, at higher densities the transfer occurs from and goes to regions closer to the branch point, consistent with the overall contraction of the star with η seen in Figure 2, and as one would expect from the general contraction of polymer chains with density. Finally, as f increases, the total monomer density transferred increases sharply, which is why $g - g_0$ grows with f in Tables 4 and 5.

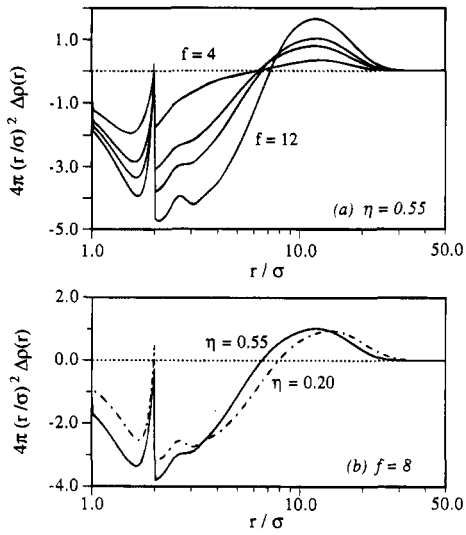

Figure 3. The difference $\Delta\rho(r)$ between the monomer density per arm of an $f \times 100$ star and the monomer density of an $N = 100$ linear chain at the same packing fraction (see eq 22). Distance r is measured from the star branch point or the end of the linear chain. Shown in (a): $\Delta\rho(r)$ for $f = 4$, 6, 8, and 12 at fixed density. Shown in (b): $\Delta\rho(r)$ for an $f = 8$ star at a low and a high density.

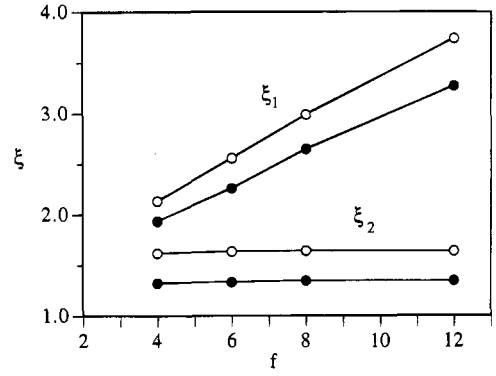

Figure 4. Local aspect ratio or persistence length ξ, averaged over the core (ξ_1) or corona (ξ_2) sites of each arm, for $f \times 100$ stars at low density ($\eta = 0.20$, open circles) and high density ($\eta = 0.55$, filled circles). For comparison some persistence lengths for linear chains of the same model, using the same theory, are 1.55 ($N = 100$, $\eta = 0.20$), 1.30 ($N = 100$, $\eta = 0.55$), 1.59 ($n = 200$, $\eta = 0.20$), and 1.32 ($N = 200$, $\eta = 0.55$).

Intuition suggests that the cause of this transfer of density is that the arms near the branch point become stretched and fill space less efficiently. Figure 4 confirms this. Shown in this figure is the local aspect ratio or persistence length ξ of the arm in the core (ξ_1) and corona (ξ_2) regions. ξ_1 is always significantly larger than ξ_2, and the ratio ξ_1/ξ_2 grows with f. This ratio also happens to grow with η, because, while the value of ξ_1 decreases with η, it does not do so by as large a fraction as the value of ξ_2. The absolute value of ξ_2 is not far at high densities from the persistence length $\xi_0 = 1.33$ of a linear chain that is ideal in the same sense as the ideal star defined at the end of section III.B.

In Figure 5 we show the variation of ξ_1 and ξ_2 with N_a for a fixed $f = 8$. Although ξ_2 appears to quickly reach a limiting value, ξ_1 continues to grow throughout the range of N_a shown. The size N_1 of the stretched core region also shows no sign of reaching a limiting value by $N_a = 1600$, so that the mean square end-to-end distance of the core region R_1^2 grows steadily across the entire range $100 \le N_a \le 1600$, as shown in Figure 6. An apparent scaling of $R_1^2 \sim N_a^{1/3}$ can be extracted

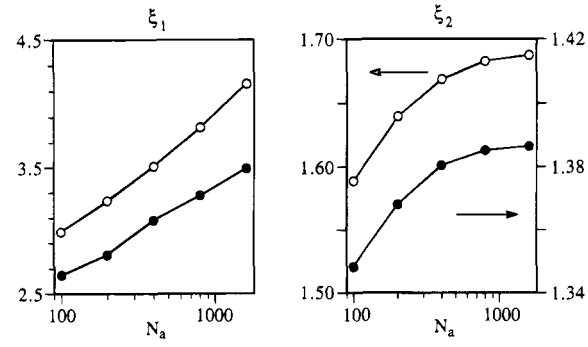

Figure 5. Local aspect ratio or persistence length ξ, averaged over the core (ξ_1) or corona (ξ_2) sites of each arm, for $8 \times N_a$ stars ($100 \le N_a \le 1600$) at low density ($\eta = 0.20$, open circles) and high density ($\eta = 0.55$, filled circles). For comparison some persistence lengths for linear chains of the same model, using the same theory, are 1.55 ($N = 100$, $\eta = 0.20$), 1.30 ($N = 100$, $\eta = 0.55$), 1.65 ($n = 1600$, $\eta = 0.20$), and 1.40 ($N = 1600$, $\eta = 0.55$).

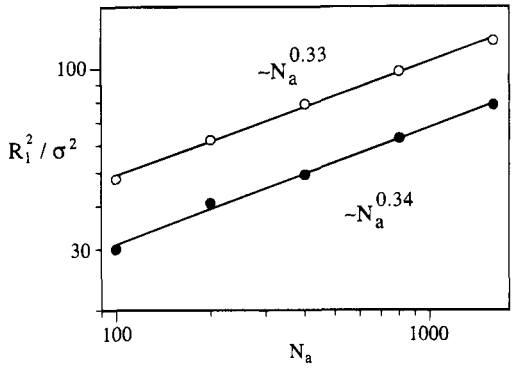

Figure 6. Mean square end-to-end distances of the core region of $8 \times N_a$ stars at low density ($\eta = 0.20$, open circles) and high density ($\eta = 0.55$, filled circles). Shown also are the results of fitting a power law to the dependence of R_1^2 on N_a.

from Figure 6, so that the ratio of core to total arm end-to-end distance, R_1^2/R^2, could be said to scale roughly as $N_a^{-2/3}$. The *relative* degree of stretching of the core regions, as measured by this ratio, appears therefore to be a slowly decaying finite-size effect, which would vanish in the $N_a \to \infty$ limit.

What causes the star arms to stretch preferentially in the core region? At low polymer concentration ($\eta \to 0$) the answer is clearly the extra long-range excluded-volume interactions the core experiences from the crowding together of the star arms near the branch point. In the formalism of our theory, the free energy F of a "test" star in the solution has a nonideal component F_{exc} from excluded-volume interactions that can be decreased by stretching the core. Doing so increases the ideal component F_{ideal} and an equilibrium degree of chain stretching is reached when the differential decrease in F_{exc} on further stretching just compensates for the differential increase in F_{ideal}.

However, at high polymer concentration the long-range excluded-volume interactions are normally screened by intermolecular interactions. In our formalism any change in F_{exc} induced by changing conformation is largely canceled by an accompanying change in F_{solv}. Why then should there be *any* stretching of the core at high density? In brief the answer to this is in two parts: first, screening of long-range excluded-volume interactions is less effective for core sites than for corona sites because the corona shields the core from the intermolecular interactions that cause screening.

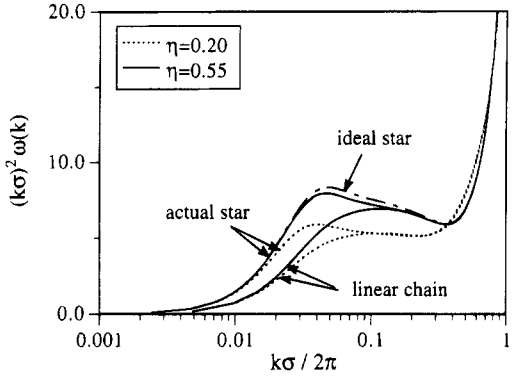

Figure 7. Average intramolecular pair correlation function $\omega(k)$ for a 4 × 100 star, shown in Kratky form. The dashed curve labeled "ideal star" shows the density-independent conformation of a star with $\epsilon_1^{eq} = \epsilon_2^{eq} = \epsilon_0 = 0$. The curves labeled "linear chain" show $\omega(k)$ for a 2 × 100 star (i.e., linear 200-mer).

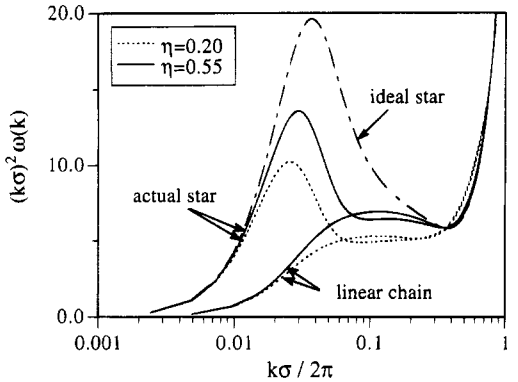

Figure 8. Average intramolecular pair correlation function $\omega(k)$ for a 12 × 100 star, shown in Kratky form. The meaning of the labels is as in Figure 7. From comparison of this figure to Figure 7 it is apparent that the degree to which the actual star differs from the ideal star increases strongly with arm number.

Second, most of the driving force for core expansion is "nonlocal," in the sense that it originates not in excluded-volume interactions between the core sites themselves, but between core and corona sites, and between corona sites on different arms. (This is in distinct contrast to the situation for linear chains: the driving force for expansion of the "core" of two-arm "stars" is dominated by forces of "local" origin, i.e. by the interactions among "core" sites themselves.) Screening of excluded-volume forces is inherently more efficient between sites that are already well-correlated by being connected by short stretches of polymer backbone. Conversely, screening of excluded-volume forces is *less* efficient between pairs of sites on different arms, or where one site is in the corona and one is in the core, since sites such as these are only weakly correlated by the long stretches of polymer backbone that connect them. We will present a detailed explanation of these statements in section IV.C.

Figures 7 and 8 show Kratky plots of the average intramolecular structure factor $\omega(k) = N^{-1} \sum_{\alpha,\beta} \omega_{\alpha\beta}(k)$. In these two figures we have shown for comparison $k^2\omega(k)$ for 2 × 100 "stars" (i.e. linear 200-mers), calculated self-consistently with the same theory. We have also shown $k^2\omega(k)$ for the ideal star as defined at the very end of section III.B. Note the characteristic small-k peak in $k^2\omega(k)$ in the star curves, the signature of the increased connectivity of the star with respect to the linear chain. The actual stars show a significantly

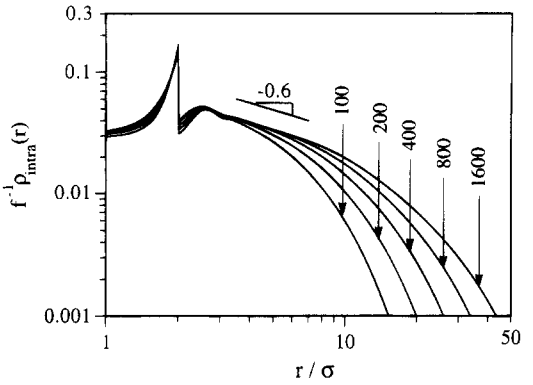

Figure 9. Log–log plot of the monomer density per arm of 8 × N_a stars at $\eta = 0.55$ as a function of distance r from the branch point. Each curve is labeled with the value of N_a, and the arrows of the labels point to the value of R_g/σ in each case. The short line shows the closest apparent scaling law exponent. The Daoud–Cotton model prediction for this exponent is −1.

smaller low-k peak than do the ideal stars, because the crowding of monomers due to increased connectivity that causes this peak is partially canceled by the nonideal stretching of the star arms.

A. Comparison with Other Theories. The most widely studied non-Gaussian theoretical model of star conformations is that of Daoud and Cotton,[18] which is based on the "blob" model of semidilute linear chain solutions and on the assumption that each arm of the star, as it radiates away from the branch point, is strictly confined to within a solid angle $4\pi/f$ by the other arms. It is the predictions the Daoud–Cotton model makes for *dilute* good-solvent solution that have received the most attention. However, the model also makes scaling predictions for Θ-solutions, and, as Horton *et al.*[14] and Boothroyd and Ball[32] have argued, these predictions should in principle apply equally to the melt, since they are based only on the confinement-of-arms ansatz and ideal ($r^2 \sim n$) scaling of the size r^2 of segments of the chain with length n. It is not clear that the lower limit of arm-number f for which the Daoud–Cotton model makes sense extends to the $f \leq 12$ stars we study, but nevertheless, the comparison of our results to the Daoud–Cotton predictions is of interest. Those predictions are as follows:

$$\rho_{intra}(r) \sim f^{1/2} r^{-1} \tag{23}$$

for the intramolecular (on the same star) monomer density as a function of distance r from the branch point, and,

$$R_g^2 \sim f^{1/2} N_a^1 \tag{24}$$

for the size of the star.

Figure 9 shows $f^{-1}\rho_{intra}(r)$, that is the intramolecular monomer density *per arm*, for 8 × N_a stars at high density ($\eta = 0.55$) on a log–log plot. One could interpret this figure as showing the development of an intermediate power-law scaling regime as N_a increases, but the evidence would have to be considered marginal in our opinion. Of course, scaling behavior might be concealed by large "crossover" effects, since the local (σ) and global (R_g) length (scales) of the star are separated by only a factor of 36 in the largest star contributing to Figure 9. This separation, while certainly comparable to experimental systems, may not yet be enough to allow the clear dominance of some intermediate length scale such

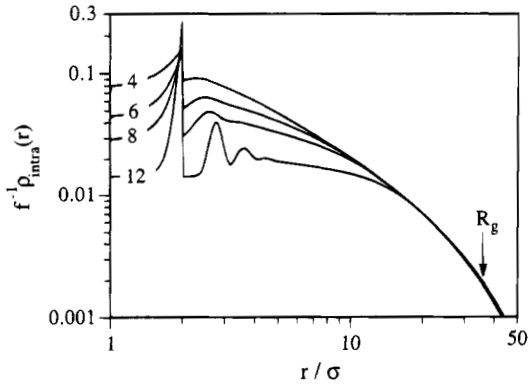

Figure 10. Monomer density per arm of $f \times 1600$ stars at $\eta = 0.55$ as a function of distance r from the branch point. Each curve is labeled with the value of f. The arrow indicates R_g/σ, which is at essentially the same place on the scale of this plot for all values of f.

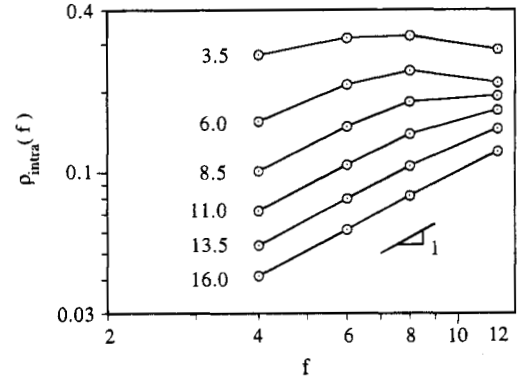

Figure 11. Monomer density of $f \times 1600$ stars at $\eta = 0.55$ as a function of arm number f, at various values of distance from the branch point r. Each curve is labeled with the value of r/σ at which it is drawn. At large r the monomer density scales as f^1, which is just the prediction of any independent-arm model.

as the proposed local "blob" size in the Daoud–Cotton model. Exactly how much larger than σ we must make R_g to clearly observe (or rule out) scaling behavior cannot be determined from scaling arguments themselves, unfortunately.[63]

Figure 10 shows $f^{-1}\rho_{intra}(r)$ for $f \times 1600$ stars. $f^{-1}\rho_{intra}$ is dependent of f for any ideal model of the star—such as the Gaussian-star model—in which the arms do not strongly perturb each others' conformation by their presence, and, as can be seen from this figure, we find this for our model stars on the length scale of R_g and larger. Given the relatively few (<12) number of arms on these stars, this is not unexpected, and, indeed, one would guess that for finite f this result would always obtain at high concentration for large enough N_a.

At smaller r we find that $f^{-1}\rho_{intra}(r)$ varies with f, which is inconsistent with any independent-arm model. However, any exponent resulting from a power-law fit to the curves in this region would vary with f, which is also inconsistent with the Daoud–Cotton model. Equation 23 gives $\rho_{intra} \sim r^{-1}$ for all f, while the apparent power-law behavior of $\rho_{intra}(r)$ at intermediate r seen in Figure 10 varies from about $r^{-1.2}$ ($f = 4$) to $r^{-0.3}$ ($f = 12$).

If ρ_{intra} is considered as a function of f at fixed values of r to illuminate its f dependence, as in Figure 11, the closest apparent intermediate region power-law behavior we can find varies between about $f^{0.0}$ and (exactly) f^1, depending on the particular value of r chosen. The physical origins of this variation are two: First, the increase of total molecular weight $N \approx fN_a$ with f tends to increase $\rho_{intra}(r)$ with f at any fixed r. This would lead to a positive scaling exponent. Competing against this "ideal" effect, however, is the transfer of monomer density from the inner to the outer regions of the star illustrated in Figure 3. This transfer increases with f; that is, $\rho_{intra}(r)$ at small r is *increasingly depleted* by monomer density transfer as f increases. This "nonideal" effect would tend to lead to a negative scaling exponent. The combination of "ideal" and "nonideal" effects gives the actual scaling exponents seen, nearly 0 at small r and exactly 1 at large r. The linear scaling of ρ_{intra} with f that emerges in Figure 11 at large $r \sim R_g$ is the prediction of all independent-arm models, and occurs for the same relatively trivial reason as the independence of f seen in $f^{-1}\rho_{intra}(r)$ for large r in Figure 9.

Turning to the size of stars, we note that the Gaussian-star model predicts $g \sim f^{-1}N_a^0$, while the Daoud–Cotton model (eq 24) predicts $g \sim f^{-1/2}N_a^0$. What we find (Tables 3 and 5) is $g \sim f^{-0.64}N_a^{-0.04}$, which is not consistent with either model. The N_a dependence is very weak, and may perhaps vanish in the $N_a \to \infty$ limit. The f dependence rather suggests a degree of avoidance by the arms of each other that is "between", in some sense, that proposed by the Gaussian model (none) and that proposed by the Daoud–Cotton model (complete). A conclusion that our theory displays a "partial" avoidance by star arms of each other in the melt would therefore be an accurate statement, but we emphasize that it would be a statement about the results of and not the assumptions underlying our calculations.

Boothroyd and Ball have classified those theoretical models of star conformation in the melt that allow for stretching of the arms.[32] They define c^2 thus,

$$R_g^2(f,N_a) = \tilde{R}_g^2(f,N_a) + c^2 \qquad (25)$$

where $\tilde{R}_g^2$ is the radius of gyration of some independent-arm model, e.g. the Gaussian-star model. Then they define as class 1 those models that do not predict a dependence of c^2 on N_a and as class 2 those models that do. To class 1 belong, for example, "wormlike"[64] and R.I.S.[11,65] stars. Boothroyd and Ball proved that *any* model in which arm stretching has a purely "local" origin—i.e. does not arise from any interactions involving the outer regions of the arms—must belong to class 1 in the long-arm limit. To illustrate class 2 Boothroyd and Ball constructed a simple phenomenological model in which a star consists of Gaussian chains, but all monomers in the corona region of the star arms are excluded from coming closer than some fixed distance r_0 from the branch point. They showed that this model predicts $c^2 \sim N_a^{1/2}$ in the limit $r_0 \ll R_g$. The exclusion-zone idea has seen considerable further development in the context of the very-many-arm star, or polymer brush formed on a tightly curved surface,[23,25] and characteristics of an exclusion zone for the arm-ends in this context have been derived by self-consistent-field theories assuming ground-state dominance.[25]

Our theory of the star at high density belongs to Boothroyd and Ball's class 2, as implied by the significant N_a dependence of c^2 shown in Tables 2 and 3, and as will become more explicitly apparent in section IV.C. Indeed, the apparent dependence of c^2 on N_a that we find ($c^2 \sim N_a^{0.42}$ for $f = 8$ stars at $\eta = 0.55$) is not far from the $N_a^{1/2}$ dependence of the simple "corona exclusion zone" model. If we work out r_0 using eq 5 of ref

32, we find a value for the "size" r_0 of the exclusion zone that changes weakly with N_a ($r_0 \sim N_a^{-0.09}$), and strongly with f ($r_0 \sim f^{1.7}$). Note that ref 32 proposes $r_0 \sim f^{\nu} N_a^0$, with $1 < \nu < 2$.

A sharply-defined zone of *complete* exclusion of the corona is not realistic at the detailed level of description of star conformation we have adopted, and, indeed, such a sharp zone has never turned up in computer simulations of the same model.[30] But the exclusion zone, at least in the few-arm limit, could certainly be considered to be a coarse-grained, "step-function"-like approximation to the transfer of monomer density outward seen in Figure 3. If we interpret the exclusion zone in this way, as being rather "soft" and fuzzy-edged, then it appears reasonable to say that our results are consistent with this model of star conformation. Note that since we do not assume but rather predict arm stretching and the associated transfer of monomer density outward, we can inquire into the microscopic physical origins of these effects, as we will do in section IV.C.

B. Comparison with Experiment. Small-angle neutron scattering (SANS) experiments have measured the size of star-branched polybutadiene in the bulk melt.[14] As does our theoretical work, the results of these experiments suggest that the stars are swollen in the melt, that is, that the size of the star is greater than what an independent-arm model would predict. Reference 14 reported values of c^2, with R_g^2 in eq 25 defined as the measured radius of gyration and $\tilde{R}_g^2$ defined as the radius of gyration of a hypothetical star of independent arms, where the characteristics of the arms (C_∞ in particular) were those of linear polybutadiene. c^2 was found to depend strongly on f, which is inconsistent with any independent-arm model. Futhermore, c^2 was also found to increase with arm molecular weight M_w/f, which, as emphasized in both refs 14 and 32, is inconsistent with all models belonging to Boothroyd and Ball's class 1.

A detailed numerical comparison of our predictions with the experimental results of ref 14 is premature, because we have made no attempt to choose parameters of the model star solution that are consistent with the chemical bonding structure of polybutadiene (e.g. σ should be significantly less than b, ϵ_0 should be much greater than zero, and a bare torsional potential should be introduced). But looking nevertheless at the general trends, from Table 1 of ref 14 we extract the widest series in arm molecular weight with fixed arm number (samples S12A through S12E, for which $f = 12$ and $M_w/f = 746$ through 15 500) and find $c^2 \sim N_a^{0.49}$, which might be compared with our theoretical prediction of $c^2 \sim N_a^{0.42}$ for $8 \times N_a$ stars at $\eta = 0.55$. For the widest series in arm number with arm molecular weight almost fixed (samples S3B, S4A, and S12C for which $f = 3$, 4, and 12 and $M_w/f = 2270$, 2380, and 2360, respectively) we find $c^2 \sim f^{2.4}$, which might be compared with our prediction of $c^2 \sim f^{1.9}$ for $f \times 100$ stars at $\eta = 0.55$.

We have also made a crude mapping of our simple model onto the real polybutadiene stars in the experiments of Horton *et al.*, as follows: First, we set the number of sites in our model stars equal to the number of backbone carbon atoms in the polybutadiene stars. Second, we set the site diameter σ in our model equal to a rough value of 4.0 Å for the effective diameter of a CH_2 group. Finally, since we only have calculations for $f = 8$ stars, and not for the $f = 12$ stars which form the widest series in arm molecular weight in ref 14, we scale the R_g^2 values we calculate for $f = 8$ stars by eq 14 to get approximate R_g^2 values for $f = 12$ stars. A comparison of our final theoretical predictions for c^2—which are entirely free of adjustable parameters—with the experimental measurements is shown in Figure 12.

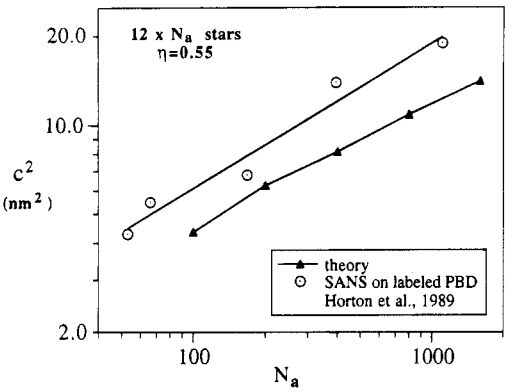

Figure 12. Swelling measure c^2 as measured experimentally[14] (circles) and as predicted theoretically (triangles). The line through the circles is a least-squares fit. The line through the triangles simply joins the symbols.

We note in concluding this section that, by using deuterated/hydrogenated diblock copolymers as the arms of a star molecule, Lantman *et al.* have been able to measure directly by SANS the degree of stretching (i.e. departure from the bulk relationship between R_g and M_w) in various regions of the star.[15] In good solvent at very dilute concentrations they report stretching of the arms near the branch point. Measurements of arm stretching using this same system in concentrated solution and the melt could more directly test some of our predictions.

C. Microscopic Origin of Nonideal Star Swelling. We now return to examine in microscopic detail why the star arms stretch preferentially in the core region even at high polymer concentration. First we define the thermodynamic forces the test star core or corona experiences, as minus the differential change of the test star free energy F that results from a differential change in the appropriate conformational parameter, e.g. for the stretching forces on the core,

$$\tilde{f}_{ideal}(\epsilon_1) \equiv -\left(\frac{\partial F_{ideal}}{\partial \epsilon_1}\right)_{\epsilon_2, N_1}$$

$$\tilde{f}_{exc}(\epsilon_1) \equiv -\left(\frac{\partial F_{exc}}{\partial \epsilon_1}\right)_{\epsilon_2, N_1} \qquad (26)$$

$$\tilde{f}_{solv}(\epsilon_1) \equiv -\left(\frac{\partial F_{solv}}{\partial \epsilon_1}\right)_{\epsilon_2, N_1}$$

Similar definitions apply for the stretching forces on the corona, giving derivatives with respect to ϵ_2, and for the forces on the size of the core, giving derivatives with respect to N_1. The equilibrium condition that F be minimized is then equivalent to the condition that the net force on each conformational parameter be zero,

$$\tilde{f}_{exc}(\epsilon_1^{eq}) + \tilde{f}_{solv}(\epsilon_1^{eq}) + \tilde{f}_{ideal}(\epsilon_1^{eq}) = 0 \qquad (27)$$

with similar requirements for ϵ_2^{eq} and N_1^{eq}. We will work with the stretching forces normalized to a per-site basis, e.g. $f_{exc}(\epsilon_1) = N_1^{-1}\tilde{f}_{exc}(\epsilon_1)$ and $f_{solv}(\epsilon_2) = N_2^{-1}\tilde{f}_{solv}(\epsilon_2)$, so that by construction $f_{ideal}(\epsilon_1) = f_{ideal}(\epsilon_2)$.

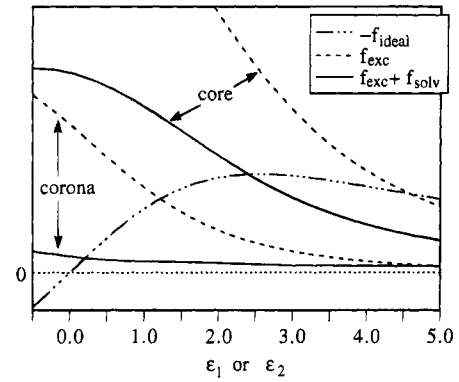

Figure 13. Thermodynamic stretching forces per unit site (cf. eq 26) on the core and corona of an 8 × 100 "test" star inserted into an $\eta = 0.55$ melt of other 8 × 100 stars. The solvating stars have the equilibrium conformational parameters given in Table 1. The test star parameter that is *not* varied in each of the curves above (e.g., ϵ_2 in the case of $f_{exc}(\epsilon_1)$) is held fixed at zero. $N_1 = N_1^{eq} = 10$ for all curves. No vertical scale is shown because the units are dimensionless and the absolute numerical values of the forces have no particular significance.

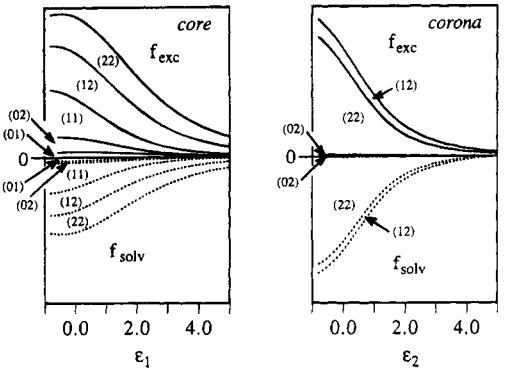

Figure 14. Origin by type of site-pair interaction of the nonideal forces on core and corona of the 8 × 100 test star shown in Figure 13. Both the f_{exc} curves, reproduced from Figure 13, and the f_{solv} curves are divided into strips showing the contributions from each of the six different possible types of site-pair interactions. The width of each strip shows the size of the contribution; i.e., the vertical distance between the two curves bounding the strip marked "(11)" under the $f_{exc}(\epsilon_1)$ curve shows the contribution to $f_{exc}(\epsilon_1)$ from core site–core site interactions. Contributions not explicitly shown, e.g., $f^{(00)}(\epsilon_1)$, $f^{(01)}(\epsilon_2)$, etc., are zero.

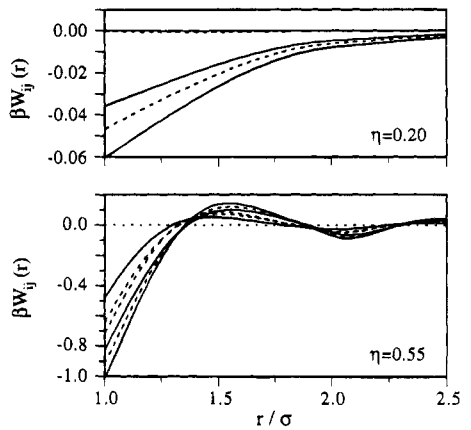

Figure 15. The six pair components W_{ij} ($\{i, j\} = 0, 1, 2$) of the solvation potential W acting on the 8 × 100 test star shown in Figure 13. In each subfigure the three "diagonal" components W_{ii}, $i = 0, 1, 2$, are drawn with solid lines and the three "off-diagonal" components W_{ij}, $j \neq i$, are drawn with dashed lines. The strengths of the components at $r = \sigma$ are, from weakest (least negative) to strongest (most negative), {0, 0}, {0, 1}, {0, 2}, {1, 1}, {1, 2}, and {2, 2}, respectively. Only the three strongest W_{ij} (W_{11}, W_{12}, and W_{22}) can be discerned on the low-density plot—the others are nearly zero.

Shown in Figure 13 are the stretching forces per site on the core and corona (at fixed $N_1 = N_1^{eq}$) for an 8 × 100 test star inserted into an $\eta = 0.55$ "melt" of other 8 × 100 stars. The conformation of the other stars is described by $\{\epsilon_1^{eq}, \epsilon_2^{eq}, N_1^{eq}\}$ as given in Table 1. In this figure the intersections of the curves for the net nonideal force, $f_{nonid} = f_{exc} + f_{solv}$, with the curve for the ideal force, $-f_{ideal}$, mark the values of ϵ_1^{eq} and ϵ_2^{eq}. As $\eta \to 0$ f_{solv} vanishes, and the only contribution to f_{nonid} is f_{exc}. As anticipated earlier, $f_{exc}(\epsilon_1) \gg f_{exc}(\epsilon_2)$, and this is exactly why $\epsilon_1^{eq} > \epsilon_2^{eq}$ in the $\eta \to 0$ limit.[66]

As η increases to 0.55, the screening of excluded-volume forces, or equivalently the increasing strength of the compressive solvation-potential forces, leads to a reduction in f_{nonid}. The net nonideal force on the corona declines nearly to zero, consistent with the general principle of polymer ideality in the melt, but the net nonideal force on the core does not decline to zero. This observation returns us to the question asked before: why *doesn't* the increase of $f_{solv}(\epsilon_1)$ with η, relative to $f_{exc}(\epsilon_1)$, match the increase in $f_{solv}(\epsilon_2)$ with η, relative to $f_{exc}(\epsilon_2)$? In other words, why does ideality *fail* to develop at high polymer concentration for the core when it *does* develop for the corona?

Our first step in answering this question is to pick out the contributions to F from the interactions among and between the various types of sites. We calculate separately the six types of sums over site pairs $\{\alpha, \beta\}$ on the right-hand side of eq 12 for which the site types of $\{\alpha, \beta\}$ are {0, 0}, {0, 1}, {0, 2}, {1, 1}, {1, 2}, and {2, 2}. We label the resulting contributions to F as $F^{(ij)}$ and to f as $f^{(ij)}$. For example, the contribution to the stretching force on the core from the excluded-volume interactions among core sites is $f_{exc}^{(11)}(\epsilon_1)$, while $f_{solv}^{(12)}(\epsilon_2)$ represents the contribution to the stretching force on the corona from solvation-potential interactions between core and corona sites.

Shown in Figure 14 are all the nonzero contributions to the nonideal forces on the core and corona. Interestingly, the forces on the core are dominated by what we might call "nonlocal" contributions: the contribution from interactions between core and corona sites $[f_{exc}^{(12)}(\epsilon_1)$ and $f_{solv}^{(12)}(\epsilon_1)]$, and the contribution from interactions between corona sites on different arms $[f_{exc}^{(22)}(\epsilon_1)$ and $f_{solv}^{(22)}(\epsilon_1)]$. The interactions between the core sites themselves actually make relatively minor "local" contributions $[f_{exc}^{(11)}(\epsilon_1)$ and $f_{solv}^{(11)}(\epsilon_1)]$. Thus the proper conceptual origin of star core expansion is not so much that the core regions in avoiding each other "push" the corona regions outward, but rather that the corona regions "pull" the core regions taut in order to avoid both themselves and the core regions. Within this conceptual framework it is clear our theory belongs to Boothroyd and Ball's class 2. It is also then straightforward to rationalize the increase of core stiffening with arm *length* seen in Figure 5, and the increase in star swelling seen in Tables 2 and 3 (and in experiment;[14] see section IV.B): When the arms become longer, the "nonlocal" forces from corona–corona and corona–core interactions increase and the "pulling" force on the core gets larger.

Figure 15 shows the solvation potentials that govern the $f_{solv}^{(ij)}$ for the 8 × 100 star solution at $\eta = 0.20$ and $\eta = 0.55$. What is apparent is that the solvation potentials the core sites experience, W_{01}, W_{11}, and W_{12}, are

not as strong as the most important solvation potential the corona sites experience, W_{22}. This is the first part of why ideality fails to develop in the core. Figure 16 shows the change in the net nonideal force on the test star core when all the W_{ij} are set equal to W_{22}. There is a significant drop, particularly in the contribution from the interactions among core sites themselves $[f^{(11)}_{\text{nonid}}(\epsilon_1)]$. This contribution in fact becomes comparable to the equivalent contribution to corona stretching by interactions among corona sites $[f^{(22)}_{\text{nonid}}(\epsilon_2)]$.

That the inner solvation potentials are weaker than the outer simply expresses the physical fact that the corona shields the core from intermolecular interactions. From eq 8 it can be seen that the strength of the solvation potentials [e.g. $W_{\alpha\beta}(k\rightarrow 0)$] is directly proportional to the strength of the direct intermolecular correlation functions [i.e. $W(k\rightarrow 0) \propto c^2(k\rightarrow 0)$], so that weak solvation potentials result from weak direct correlation functions. And c measures by definition intermolecular interaction; the probability of contact between sites α and β on different molecules, for example, is proportional to $g_{\alpha\beta}(\sigma)$, and this quantity decreases with decreasing $|c_{\alpha\beta}(k\rightarrow 0)|$. Thus weak direct correlation functions result from (among other things) low probabilities of intermolecular contact, as expressed by deep correlation holes. It will be shown in a following paper[44] that the core sites do indeed have much deeper correlation holes than do the corona sites, as one would expect from the fact that the former are on average "buried" deeper within the star (e.g. the average intramolecular monomer density around a core site is higher than around a corona site).

The contribution to the net nonideal force from core–corona interactions does not change dramatically going from the left to right sides of Figure 16, and the contribution from corona–corona interactions does not change at all (it can't because $f^{(22)}_{\text{solv}}(\epsilon_1)$ depends only on W_{22}). The reason for these large contributions to the core stretching force does not therefore lie in the strength of the solvation potentials. Instead it lies in the differing intrinsic effectiveness of the solvation potential in canceling excluded-volume interactions for sites that are strongly and weakly correlated. To explain this we first note that the nonideal free energy of the test star is built up in eq 12 principally out of terms of this form,

$$F^{(\alpha\beta)}_{\text{nonid}} = -\int \mathrm{d}^3 r\, \omega_{\alpha\beta}(r) f(r)$$

$$f(r) = \exp\{-\beta[u_{\text{HS}}(r) + W(r)]\} - 1 \qquad (28)$$

This form is similar to the terms in a mean-field two-body approximation to the free energy,[61,63,67] the difference being the weighting of the Mayer f-function by the probability $\omega_{\alpha\beta}(r)$ that the two sites are a distance r apart. If this weighting were to become independent of r, eq 28 would reduce to the mean-field form of a probability of α–β contact multiplied by an excluded-volume parameter v, with v essentially the monomeric second-virial coefficient, $v = -\int \mathrm{d}^3 r\, f(r)$.

In Figure 17 we have shown the $\omega_{\alpha\beta}(r)$ for two sites that are 3 and 20 backbone bonds apart. Superimposed on these curves is a generic polymeric f-function (that for the corona of the 8 × 100 star at $\eta = 0.55$), so that one can readily see for each case which portions of the f-function are weighted most by $\omega_{\alpha\beta}(r)$ in eq 28. The short-chain $\omega_{\alpha\beta}(r)$ is strongly peaked at small values of r, and this peak moves rapidly outward with increasing

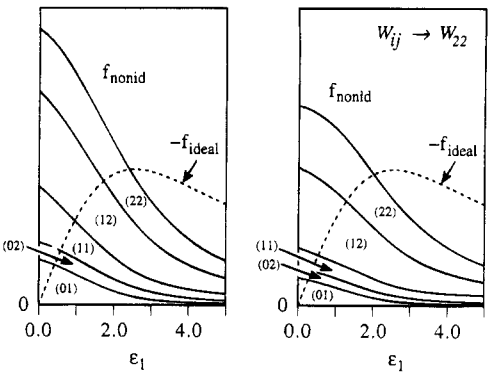

Figure 16. Net nonideal forces on the core of the 8 × 100 test star shown in Figure 13. As in Figure 14 the total curve is divided into strips showing the contributions from the different types of pair interactions. On the left-hand side of this figure are shown the actual contributions to the actual $f_{\text{nonid}}(\epsilon_1)$. On the right-hand side are shown the contributions to $f_{\text{nonid}}(\epsilon_1)$ if all the solvation pair components (shown in Figure 15) are set equal to W_{22}.

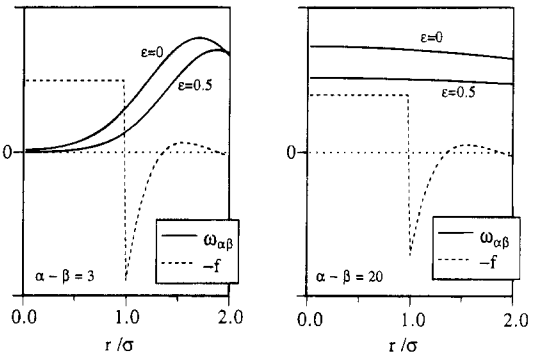

Figure 17. Components of eq 28, the contribution to the nonideal free energy, for two sites α and β joined by short and long strands of polymer chain. $\omega_{\alpha\beta}(r)$ is the probability density of finding the sites r apart. $f(r)$ is a generic Mayer f-function for their interaction. ϵ measures the stiffness of the chain joining the sites. While the two $\omega_{\alpha\beta}$ curves in each subfigure are on the same scale, they are not on the same scale as the $-f(r)$ curve, nor are the curves for the long-chain subfigure on the same scale as those for the short-chain figure. All scales have been chosen to emphasize the *shape* of the curves and how this changes with ϵ.

chain stiffness. By contrast the long-chain $\omega_{\alpha\beta}(r)$ is nearly flat over the range shown, indicating of course a much weaker correlation of the location of β with that of α. The principal result of increasing the stiffness of the intervening chain in this case is simply to lower the general magnitude of $\omega_{\alpha\beta}(r)$; that is, the probability of close approach of α and β is reduced without the spatial *distribution* of that probability *in the range of* $f(r)$ being significantly altered.

The nonideal stretching force on the connecting chain generated by the excluded-volume interaction between sites α and β, $f^{(\alpha\beta)}_{\text{exc}}(\epsilon)$, is given from eq 28 essentially by the change, when the chain is stretched, in the weighting of the excluded-volume domain of the f-function ($r < \sigma$). Similarly, the nonideal stretching force generated by the solvation-potential interaction, $f^{(\alpha\beta)}_{\text{solv}}(\epsilon)$, comes from the change in the weighting of the solvation-potential domain of the f-function (roughly $\sigma \le r < 1.5\sigma$). Figure 17 suggests that the short-chain $\omega_{\alpha\beta}(r)$ changes more in the solvation-potential region, relative to the change in the excluded-volume region, than does the long-chain $\omega_{\alpha\beta}(r)$. Thus the magnitude of $f^{(\alpha\beta)}_{\text{solv}}(\epsilon)$ should be a larger fraction of the magnitude of $f^{(\alpha\beta)}_{\text{exc}}(\epsilon)$ for the short chain than for the long chain. This is confirmed

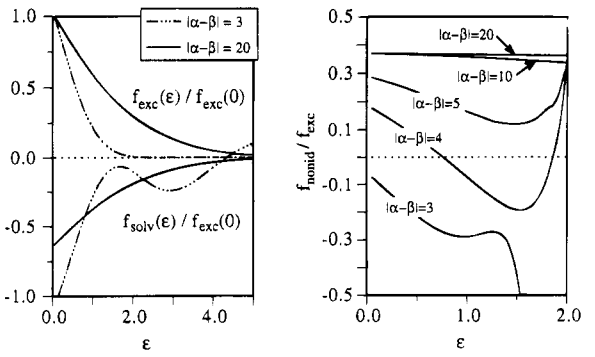

Figure 18. Nonideal forces generated by the interaction of two sites joined by short and long strands of polymer. The right side of this figure could also be interpreted, as discussed in the text, as an effective excluded volume parameter $\tilde{v}_{\alpha\beta}(\epsilon,\eta)$ measured in terms of an effective bare excluded volume $\tilde{v}_{\alpha\beta}(\epsilon;\eta\to 0)$. Note the complete disappearance of f_{exc} for $|\alpha-\beta| = 3$ as $\epsilon > 2.0$ on the left, caused by $\omega_{\alpha\beta}(r<\sigma) \to 0$. This is not matched by a disappearance of f_{solv} at the same ϵ. This is why the corresponding f_{nonid}/f_{exc} curve on the right diverges as it approaches $\epsilon = 2.0$. The divergences (at higher ϵ) of the $|\alpha-\beta| = 4$, 5 curves have the same origin, the direction of the divergence depending on whether $f_{solv}(\epsilon)$ is positive or negative. For large $|\alpha-\beta|$, however, $\omega_{\alpha\beta}(r<\sigma) \neq 0$ even for very large ϵ—the sites remain poorly correlated, if on the average further apart—and so $f_{exc} > 0$ always.

by the left-hand side of Figure 18, where we show the result of explicitly calculating $f_{exc}^{(\alpha\beta)}(\epsilon)$ and $f_{solv}^{(\alpha\beta)}(\epsilon)$, using the f-function shown in Figure 17.

We conclude from Figure 18 that the cancellation of $f_{exc}^{(\alpha\beta)}(\epsilon)$ by $f_{solv}^{(\alpha\beta)}(\epsilon)$, or, equivalently, the screening of long-range excluded-volume interactions, is inherently more efficient for sites that are well-correlated by virtue of being connected with shorter stretches of polymer backbone. The right-hand side of Figure 18 shows the fraction of the excluded-volume force that remains unscreened at high density for sites separated by varying lengths of backbone chain. As we mentioned above, the usual mean-field formula for the contribution by a site pair to the free energy is a probability of contact times an excluded-volume parameter v. In this case the force for expansion is just v times (minus) the differential change in contact probability with chain stretching. It is readily seen by inspecting Figure 17 that this is exactly what eq 28 will reduce to in the limit that the sites become nearly uncorrelated, i.e.

$$f_{nonid}^{(\alpha\beta)}(\epsilon) \xrightarrow{|\alpha-\beta|\to\infty} -v\frac{\partial}{\partial\epsilon}\omega_{\alpha\beta}(r=0) \qquad (29)$$

In the same limit we also have

$$f_{exc}^{(\alpha\beta)}(\epsilon) \xrightarrow{|\alpha-\beta|\to\infty} -v_0\frac{\partial}{\partial\epsilon}\omega_{\alpha\beta}(r=0) \qquad (30)$$

where $v_0 = (4/3)\pi\sigma^3$ is the "bare" excluded volume between two monomers. Thus in the uncorrelated limit the ratio $f_{nonid}^{(\alpha\beta)}/f_{exc}^{(\alpha\beta)}$ plotted on the right-hand side of Figure 18 becomes exactly the constant second-virial-coefficient excluded-volume parameter v, measured in units of the base excluded volume v_0. This is already apparent in Figure 18 for $|\alpha-\beta| = 20$. We could extend this interpretation to *all* values of $|\alpha-\beta|$, in which case the right-hand side of Figure 18 shows an effective excluded volume parameter $\tilde{v}_{\alpha\beta}(\epsilon;\eta)$, measured in units of the effective bare excluded volume $\tilde{v}_{\alpha\beta}(\epsilon;\eta\to 0)$. $\tilde{v}_{\alpha\beta}$ contains all the influence of the changing correlation between sites that is left out of v. In the limit of uncorrelated sites $\tilde{v}_{\alpha\beta} \to v$, but in general $\tilde{v}_{\alpha\beta} < v < v_0$.

The sum of all the interactions between site pairs $\{\alpha, \beta\}$ on a typical length of linear polymer chain is dominated by short-chain terms, first because there are more of them, and second because the magnitude of the contribution to the net nonideal force dies off rapidly with $|\alpha-\beta|$ (it can be shown that $f_{exc}^{(\alpha\beta)}(\epsilon) \sim |\alpha-\beta|^{-3/2}$ in the long flexible chain limit, and $f_{solv}^{(\alpha\beta)}(\epsilon) \leq f_{exc}^{(\alpha\beta)}(\epsilon)$ in the same limit). This is the case for, e.g. $f_{nonid}^{(22)}(\epsilon_2)$, which dominates the forces on the star corona, as shown by Figure 14.

However, the interactions summed into $f_{nonid}^{(12)}(\epsilon_1)$ and $f_{nonid}^{(22)}(\epsilon_1)$ are *all* between sites that are separated by significant lengths of polymer backbone (at least $2N_1$ long). *There are no short-chain terms at all.* Hence these forces, which make the largest contribution to the force on the star core, as shown by Figure 14, exhibit typical long-chain behavior, i.e. poor screening of long-distance excluded-volume interactions. This is then the second part of the explanation for why ideality does not develop for the core to the degree it does for the corona. It may be restated in a physical and more general way as follows: the total nonideal stretching force on any small linear fragment of a polymer is the sum of "short-chain" contributions from the interaction of monomers near each other on the polymer backbone and "long-chain" contributions from the interactions of monomers well-separated along the polymer backbone. Normally the short-chain contributions dominate because there are more of them close by. Short-chain contributions are reduced at high polymer concentration more than long-chain contributions, because the higher degree of correlation between sites closely spaced along the polymer backbone leads to a more efficient screening of excluded-volume interactions. Now if a branch point occurs close to the fragment, the ratio of nearby long-chain to nearby short-chain contributions will increase (e.g. if the branch point is 5 backbone bonds away then the number of monomer pairs > 5 backbone bonds apart will increase by a factor of roughly f^2, where f is the number of branches, but the number of pairs < 5 bonds apart will change by only a factor of f). The added long-chain contributions will reduce the dominance of short-chain contributions, and a smaller reduction of the stretching forces with increasing concentration will be observed. That is, the fragment will be stretched at high concentration more than it would be were there no branch point nearby.

As a final comment we note that the most proper frame of reference in which to discuss conformational changes at high density is the many-molecule frame. But the potential surfaces are then of very high dimensionality and the extraction of their important features can be difficult. The solvation potential maps the problem of conformation at high density back onto a single-molecule problem, in principle exactly. In the case of the pairwise-additive approximation, the problem is reduced even further to that of interacting pairs of monomers. The use of the solvation potential simplifies the physical picture enormously, therefore, by integrating over solvent degrees of freedom of little direct interest, and this can aid considerably the acquisition of general physical intuition about the forces operating on large flexible molecules.

D. Conclusions. Our conclusions for the basic star-polymer model we have studied are as follows: (1) The excluded-volume interactions in the star, principally those between corona sites on different arms and between core and corona sites, serve to pull the core

regions of the star taut. These interactions are less well screened at high density than the excluded-volume interactions in the corona partly because of the weakness of the inner solvation potentials, which is caused by the lower exposure of the core to the solvating medium, and partly by the intrinsically poorer screening by the solvation potential of excluded-volume interactions between weakly correlated sites. (2) The stretching of the core leads to a transfer of monomer density from inner to outer regions of the star, which causes a swelling of the star relative to a star with independent arms. (3) The dependence of simple measures of this swelling (e.g. c^2) on f and N_a are in qualitative agreement with experiment. (4) The swelling of the star could be coarsely interpreted in the manner proposed by Boothroyd and Ball,[32] and developed more formally for the polymer brush on a curved surface, as an effective aversion (exclusion) of the distant regions of the star arms for regions near the branch point. In the paper succeeding this[44] it will be found that this effective aversion has some interesting intermolecular consequences.

The Daoud–Cotton model is not found to describe our stars very accurately. This is not surprising, as the model has been argued to hold only in the large-f limit, but it does underline the utility of a theory that can accommodate easily the experimentally-relevant small-f limit.

Although we have not—and cannot using the generating functional technique—investigated the dilute limit of star solutions,[68] our experience does suggest a different perspective on one of the primary predictions of the Daoud–Cotton star model for dilute star solutions. This prediction was that the increasing local monomer density necessarily found as one penetrates into a star polymer in dilute solution leads to an increased screening of the intramonomeric repulsion, and eventually (for large enough stars), to a regime intermediate between corona and branch point where the local chain conformation is highly compressed. That is, if one were to construct local scaling laws for the mean square end-to-end distance r^2 of small sections of length $1 \ll n \ll N_a$ of a star arm, then while one would find self-avoiding random walk scaling, $r^2 \sim n^{1.2}$, for the outer regions of the star in dilute solution, one would find ideal scaling, $r^2 \sim n$, in some inner, compressed regime.

From the perspective of our theory it is impossible to rationalize this prediction. The problem is the assumption that screening increases toward the center of the star because of the increase in local monomer density. But from the point of view of our theory the connection between screening and monomer density is *not local*. Rather the source of screening in polymer solutions is the osmotic incompressibility of the solution, which is determined by the *global* average monomer density. This appears mathematically in our theory in the dependence of the solvation potential $W(r)$—the effective attraction between monomers induced by screening—on the structure factor $S(k)$, the zero-wavevector component of which is inversely proportional to osmotic compressibility and which depends (for fixed polymer size and architecture) only on global average monomer density.

The *local* influence of osmotic incompressibility is not everywhere identical, indeed, but local monomer density does not appear to be the relevant variable. What matters is instead the degree of local solvent exposure, appearing mathematically in our theory as the dependence of the solvation potential W on the direct correlation functions $c_{\alpha\beta}$ (which are in turn connected to the intermolecular correlation functions $g_{\alpha\beta}$ by the PRISM equation). $S(k)$, i.e. the solution osmotic incompressibility, is fixed for a given global average monomer density, but as one travels into the interior of a star, the degree of solvent exposure as measured by, say $|c_{\alpha\beta}(k\rightarrow 0)|$, always decreases. Hence the degree of local exposure to the effects of solution incompressibility always decreases as well, and one would expect screening of the repulsions between monomers on the basis of exposure to solvent always to *decrease* and never to *increase*. We find as explained in section IV.C that this effect, measured by the decreasing strength of the solvation potential as one goes into the star core, is one of the reasons that our model stars always stretch more in the core than in the corona. We note that computer simulations[30] have never observed indications of an intermediate compressed region in dilute star solutions, and that an intermediate compressed regime is not consistent with the general feature of theories for polymer brushes[23–25] that forcing chains to come closer by tethering them to a surface induces stretching (only) of the chains.

V. General Conclusions

As Freed has pointed out,[63] the construction of theoretical methods capable of treating polymers of widely different chemical identity in the concentrated and melt regimes is much more difficult than in the case of the dilute and semidilute regimes. The reason is the clear importance in dense liquids of strong local interactions (e.g. packing constraints) which vary significantly with the exact chemical identity of the polymer. There is no universal solution to this problem, of course, other than perhaps a direct, many-molecule computer simulation of every system of interest at every density, pressure, etc. of interest. But the liquid-theory method we have developed here and earlier[36,37] has some general advantages: First, one may calculate most of the usual quantities of interest that describe polymer solutions—e.g. molecular size (R_g), shape, intramolecular distributions of monomer density, intermolecular pair correlations, scattering functions, etc.—at concentrations up to and including the melt. Quantities dependent on three-site correlations are not accessible with the theory.

Second, one may study the dependence of these quantities not only on generic solution parameters such as concentration but also on nonuniversal, highly system-specific parameters of the system such as monomer size, shape, bonding constraints, local chain stiffness, etc. All these parameters enter the theory directly and unambiguously through the bonding constraint on the trial conformations, the nature of the site–site interaction potential $u(r)$, or the nature of a local interaction potential such as $V_{bend}(r)$.

Third, the theory also delivers simultaneously with the conformational information the intermolecular pair correlations $g_{ij}(r)$ and partial structure factors (collective scattering functions) $S_{ij}(k)$, as will be shown more fully in the following paper.[44]

Fourth, the computational effort required by the method, while nontrivial, is much less than that required for full-scale computer simulation of the entire solution. The complete self-consistent calculation of all the properties of a large (12×1600) star at melt ($\eta = 0.55$) densities takes about a day and a half using 1/3 of an IBM RS/6000 model 370 workstation. By contrast, Grest has commented that direct many-molecule simulations of comparable systems is currently impossible.[30]

Fifth, long-wavelength properties such as $S(k)$ at low k can be calculated quite easily with the theory, while they are time-consuming to extract from computer simulation because of the large size of sample required.

And finally, as demonstrated we hope by our extended discussion in section IV.C, the solvation potential allows one to draw an intuitive, physically-oriented picture of the forces operating on polymer molecules.

As compared with some other theoretical methods used for polymer solutions, we note that the theory does not assume incompressibility (that is, the effects of density fluctuations are fully treated), that the method is "off-lattice", that the architecture and connectivity of the molecule is always exactly treated, that we do not approximate the potential of interaction between monomers with an integrable potential, and that we do not need to be in the $N \to \infty$, $f \gg 1$, or $\rho \to 0$ limits. On the other hand, the theory is not symbolic, not derived from a rigorous expansion in a small parameter, requires significant numerical calculation, and cannot easily explore the latter three limits, nor extract rigorous scaling laws for them.

Without going beyond the basic model we have defined in section II, there are interesting extensions of the work here, such as the study of star polymers with subunits distinct by reason of size, local chain stiffness or shape (star copolymers). A more conceptually distinct but equally straightforward application of the work presented here is the treatment of linear chains attached to a large central structure, which may be considered a model for sterically stabilized colloidal fluids and fluids of diblock copolymer micelles. Of particular interest in this case will be the nonideal intermolecular correlation between the macroparticles, which in our method emerges directly as $g_{00}(r)$ and which is discussed for the star model in the next paper.[44] The quantity $-k_BT \ln[g_{00}(r)]$ can be interpreted as the effective two-body potential of mean force between the macroparticles, and it can be obtained easily in highly concentration solution.

Generalizations of the theory can be made to models of polymers that are realistic by liquid-state theory standards. That is, one may build models with strongly overlapping sites, rigid bond angles or realistic local bending and torsional potentials, and multiple types of site–site interactions. Of primary interest will be, however, the development of methods to treat accurately the effects of the attractive branch of the intermonomer interactions. One possibility for this lies in using "molecular" closures[48,49] in the PRISM equation instead of "atomic" closures like eq 7.

Acknowledgment. This research was supported by the United States Department of Energy via Sandia National Laboratory CRADA No. 1078.

References and Notes

(1) Kraus, G.; Gruver, J. T. *J. Polym. Sci., Part A* **1965**, *3*, 105.
(2) Graessley, W. W.; Masuda, T.; Roovers, J. E. L.; Hadjichristidis, N. *Macromolecules* **1976**, *9*, 127.
(3) Napper, D. H. *Polymeric Stabilization of Colloidal Dispersions*; Academic Press: New York, 1983.
(4) Vagberg, L. J. M.; Cogan, K. A.; Gast, A. P. *Macromolecules* **1991**, *24*, 1670.
(5) Pispas, S.; Hadjichristidis, N.; Mays, J. W. *Macromolecules* **1994**, *27*, 6307.
(6) Stupp, S. I.; Son, S.; Lin, H. C.; Li, L. S. *Science* **1993**, *259*, 59.
(7) Utracki, L. A.; Roovers, J. *Macromolecules* **1973**, *6*, 366.
(8) Roovers, J. *Macromolecules* **1994**, *27*, 5359.
(9) Burchard, W. *Adv. Polym. Sci.* **1983**, *48*, 1.
(10) Huber, K.; Bantle, S.; Burchard, W.; Fetters, L. J. *Macromolecules* **1986**, *19*, 1404.
(11) Huber, K.; Burchard, W.; Bantle, S.; Fetters, L. J. *Polymer* **1987**, *28*, 1990.
(12) Bauer, B. J.; Fetters, L. J.; Graessley, W. W.; Hadjichristidis, N.; Quack, G. F. *Macromolecules* **1989**, *22*, 2337.
(13) Adam, M.; Fetters, L. J.; Graessley, W. W.; Witten, T. A. *Macromolecules* **1991**, *24*, 2434.
(14) Horton, J. C.; Squires, G. L.; Boothroyd, A. T.; Fetters, L. J.; Rennie, A. R.; Glinka, C. J.; Robinson, R. A. *Macromolecules* **1989**, *22*, 681.
(15) Lantman, C. W.; MacKnight, W. J.; Rennie, A. R.; Tassin, J. F.; Monnerie, L.; Fetters, L. J. *Macromolecules* **1990**, *23*, 836.
(16) Dozier, W. D.; Huang, J. S.; Fetters, L. J. *Macromolecules* **1991**, *24*, 2810.
(17) Willner, L.; Jucknische, O.; Richter, D.; Farago, B.; Fetters, L. J.; Huang, J. S. *Europhys. Lett.* **1992**, *19*, 297.
(18) Daoud, M.; Cotton, J. P. *J. Phys. (Paris)* **1982**, *43*, 531.
(19) Birshtein, T. M.; Zhulina, E. B. *Polymer* **1984**, *25*, 1453.
(20) Ohno, K.; Binder, K. *J. Chem. Phys.* **1991**, *95*, 5444, 5459.
(21) Miyake, A.; Freed, K. F. *Macromolecules* **1983**, *16*, 1228.
(22) Douglas, J. F.; Roovers, J.; Freed, K. F. *Macromolecules* **1990**, *23*, 4168.
(23) Ball, R. C.; Marko, J. F.; Milner, S. T.; Witten, T. A. *Macromolecules* **1991**, *24*, 693.
(24) Dan, N.; Tirrell, M. *Macromolecules* **1992**, *25*, 2890.
(25) Li, H.; Witten, T. A. *Macromolecules* **1994**, *27*, 449.
(26) Grest, G. S.; Kremer, K.; Witten, T. A. *Macromolecules* **1987**, *20*, 1376.
(27) Batoulis, J.; Kremer, K. *Macromolecules* **1989**, *22*, 4277.
(28) Yethiraj, A.; Hall, C. K. *J. Chem. Phys.* **1991**, *94*, 3943.
(29) Grest, G. S. *Macromolecules* **1994**, *27*, 3493.
(30) Grest, G. S.; Murat, M. *Monte Carlo and Molecular Dynamics Simulations in Polymer Science*; Binder, K., Ed.; Clarendon Press: Oxford, England, 1994.
(31) Allegra, G.; Ganazzoli, F. *Adv. Chem. Phys.* **1989**, *75*, 265.
(32) Boothroyd, A. T.; Ball, R. C. *Macromolecules* **1990**, *23*, 1729.
(33) Ganazzoli, F.; Fontelos, M. A.; Allegra, G. *Polymers* **1993**, *34*, 2615.
(34) Allegra, G.; Colombo, E.; Ganazzoli, F. *Macromolecules* **1993**, *26*, 330.
(35) Guenza, M.; Perico, A. *Macromolecules* **1993**, *26*, 4196.
(36) Grayce, C. J.; Schweizer, K. S. *J. Chem. Phys.* **1994**, *100*, 6846.
(37) Grayce, C. J.; Yethiraj, A.; Schweizer, K. S. *J. Chem. Phys.* **1994**, *100*, 6857.
(38) Grayce, C. J.; de Pablo, J. J. *J. Chem. Phys.* **1994**, *101*, 6013.
(39) Chandler, D.; Andersen, H. C. *J. Chem. Phys.* **1972**, *57*, 1930.
(40) Chandler, D. *The Liquid State of Matter: Fluids, Simple and Complex*; Montroll, E. W., Lebowitz, J. I., Eds.; North-Holland: Amsterdam, 1982; p 275.
(41) Monson, P. A.; Morriss, G. P. *Adv. Chem. Phys.* **1990**, *77*, 451.
(42) Schweizer, K. S.; Curro, J. G. *Phys. Rev. Lett.* **1987**, *58*, 246.
(43) Schweizer, K. S.; Curro, J. G. *Adv. Polym. Sci.* **1994**, *116*, 319.
(44) Grayce, C. J.; Schweizer, K. S., to be submitted to *Macromolecules*.
(45) Our form of $V_{bend}(\theta;\epsilon)$ both here and in ref 37 differs from that in ref 59 because the potential eq 1, unlike the potential in ref 59, produces reduced conformational entropy for *both* $\epsilon < 0$ and $\epsilon > 0$. This is consistent with the intuition that favoring small angles of n.n.n. bend, as $\epsilon < 0$ does, as well as favoring large angles of n.n.n. bend, as $\epsilon > 0$ does, should *both* reduce the conformational entropy relative to favoring no particular angle of bend, which $\epsilon = 0$ does.
(46) Hansen, J.-P.; McDonald, I. R. *Theory of Simple Liquids*, 2nd ed.; Academic Press: New York, 1986.
(47) Andersen, H. C.; Chandler, D.; Weeks, J. D. *Adv. Chem. Phys.* **1976**, *34*, 105.
(48) Schweizer, K. S.; Yethiraj, A. *J. Chem. Phys.* **1993**, *98*, 9053.
(49) Yethiraj, A.; Schweizer, K. S. *J. Chem. Phys.* **1993**, *98*, 9080.
(50) Hoover, W. G.; Ree, R. H. *J. Chem. Phys.* **1968**, *49*, 3609.
(51) Chandler, D.; Pratt, L. R. *J. Chem. Phys.* **1976**, *65*, 2925.
(52) Melenkevitz, J.; Schweizer, K. S.; Curro, J. G. *Macromolecules* **1993**, *26*, 6190.
(53) Melenkevitz, J.; Curro, J. G.; Schweizer, K. S. *J. Chem. Phys.* **1993**, *99*, 5571.
(54) Donley, J. P.; Curro, J. G.; McCoy, J. D. *J. Chem. Phys.* **1994**, *101*, 3205.
(55) Sen, S.; Cohen, J. M.; McCoy, J. D.; Curro, J. G. *J. Chem. Phys.* **1994**, *101*, 9010.
(56) Sen, S.; McCoy, J. D.; Nath, S. K.; Donley, J. P.; Curro, J. G. *J. Chem. Phys.* **1995**, *102*, 3431.
(57) However, W_{00} is only of academic interest, since the central sites are fixed and cannot respond to it. The academic

interest stems from the fact that W_{00} is much weaker than W_{22} (see Figure 15). That is, the attractive force induced by the solvent between two sites at the center of the star is much weaker than the solvent-induced force between two sites out in the corona. This reflects the larger exposure to the solvent of the latter. What is important is that this demonstrates that a site-*pair*wise additive solvation potential is capable of describing the fact that central sites are "buried" on average deeper in the star than corona sites. This information would seem to be intrinsically three-body information, as indeed it is, but it is nevertheless captured by the set of *two*-body potentials $W_{\alpha\beta}$ because the site indices α and β provide an "extra" coordinate. We made this assertion in a footnote to ref 36, and referred there to the results for W_{00} here as proof.

(58) Note that eq 20 of ref 37 is wrong. It should read

$$\beta W^{\mathrm{PY}}(r) = -\log[1 + N\rho \int \mathrm{d}^3r'\, \mathrm{d}^3r''\, c(|\mathbf{r} - \mathbf{r}'|)S(|\mathbf{r}' - \mathbf{r}''|)c(r'')] \quad (31)$$

Equation 21 is correct as written.

(59) Honnell, K. G.; Curro, J. G.; Schweizer, K. S. *Macromolecules* **1990**, *23*, 3496.

(60) F is not the complete test star free energy: certain contributions that do not depend on the star conformation are left out. We thank Dr. Arun Yethiraj for this observation.

(61) de Gennes, P.-G. *Scaling Concepts in Polymer Physics*; Cornell University Press: Ithaca, NY, 1979.

(62) Zimm, B. H.; Stockmayer, W. H. *J. Chem. Phys.* **1949**, *17*, 1301.

(63) Freed, K. F. *Renormalization Group Theory of Macromolecules*; John Wiley & Sons: New York, 1987.

(64) Huber, K.; Burchard, W. *Macromolecules* **1989**, *22*, 3332.

(65) Mattice, W. L. *Macromolecules* **1982**, *15*, 1633.

(66) The actual values of ϵ_1^{eq} and ϵ_2^{eq} for $\eta \to 0$ indicated by these crossings are not expected to be quantitatively accurate, due to the approximations accepted in defining F and $\tilde{V}_1$.

(67) Flory, P. J. *Principles of Polymer Chemistry*; Cornell University Press: Ithaca, NY, 1953.

(68) However, instead of minimizing F to find the equilibrium distribution of star conformations, we could computer simulate a single star in the presence of the solvation potential W (*cf.* section IV of ref 37). Doing this *would* allow us to investigate arbitrarily small densities, but we would not be able to use the three-site-type approximation introduced in section IIIA, since there would be no unambiguous way to decide which sites belong to the core and which to the corona. Without the three-site-type approximation there would then be $\mathcal{O}(N^2)$ RISM equations to solve to find the solvation potential, a considerable burden to add to the already arduous simulation of a large single star. In any event, such an approach would reduce at low polymer concentrations simply to a computer simulation of the isolated star, since the solvation potentials vanish in this limit, and comprehensive computer simulation studies of the properties of the single star have already been made (see, e.g., ref 30).

MA950951A